

# In Situ Characterization for Understanding the Degradation in Perovskite Solar Cells

Xin Meng, Xueying Tian, Shasha Zhang,\* Jing Zhou, Yiqiang Zhang, Zonghao Liu,\* and Wei Chen\*

**In the past decade, organic–inorganic hybrid perovskite solar cells (PSCs) have made unprecedented progress and recently achieved high efficiency of over 25%, comparable with commercial silicon solar cells. However, PSCs still face poor long-term stability hindering their commercial application. Because PSCs undergo severe degradation under environmental stress factors, such as moisture, heat, light, and electrical bias. Thus, exploring and evaluating the degradation pathways of perovskites and the degradation mechanisms of PSCs is quite essential. In situ diagnostic techniques can track the real-time changes of structure, morphology, and optoelectronic properties of the materials in the device during the degradation process. Herein, the progress on in situ characterization for understanding the degradation in PSCs is reviewed, including advanced characterization techniques in the aspects of electron microscopy, X-Ray, and optoelectronic spectroscopy. Besides, in situ characterization tracking the degradation process of perovskite material films from typical methylamine (MA) perovskite to formamidinium (FA)–cesium (Cs) mixed-cation perovskite and PSCs dependent on external factors is also discussed. This overview can provide a further understanding of the stability of PSCs and solve the problems on their road to commercialization. Finally, the future perspectives of in situ characterization for understanding the degradation of PSCs are provided at the end of this review.**

## 1. Introduction

Developing clean, sustainable, high-efficiency, and cheap electric energy is the key to solving the environmental problems of global warming and energy shortages. Perovskite solar cells (PSCs) have been recognized as an emerging photovoltaic technology due to

their high efficiency and low-cost characteristics since their appearance.<sup>[1–3]</sup> Since 2009, Kojima and coworkers have applied organic halide perovskite nanocrystals to solar cell research as a photosensitizer.<sup>[4]</sup> In the following 12 years, organic–inorganic hybrid PSCs' photoelectric conversion efficiency (PCE) has rapidly risen from the reported 3.8% to 25.7%.<sup>[5–8]</sup> It has surpassed the highest efficiency of 23.3% for polycrystalline silicon solar cells and is catching up with the highest efficiency of 26.7% for monocrystalline silicon solar cells.<sup>[9]</sup>

However, poor long-term stability has become a commonly recognized issue for PSCs in the coming commercial revolution. The stability of PSCs mainly contains two parts.<sup>[3]</sup> The first part is the instinct stability of perovskite material. The relatively weak lead–halogen bonds in the perovskite lattice would easily cause crystal structure and composition changes, leading to the irreversible decomposition of perovskites with volatile byproducts. In addition to the instinct instability of perovskite, the charge transport materials electrode mate-

rials in PSCs may also tend to cause additional degradation of PSCs due to the potential interfacial deterioration. The degradation of these interfacial layers also can impair the performance of PSCs. Another part is the extrinsic stability of bulk perovskite material together with these layers under the detrimental external stresses, such as heat, light, bias, and H<sub>2</sub>O/O<sub>2</sub>. The instinct

X. Meng, X. Tian, J. Zhou, Z. Liu, W. Chen  
Wuhan National Laboratory for Optoelectronics  
Huazhong University of Science and Technology  
Wuhan 430074, China  
E-mail: liuzonghao@hust.edu.cn; wnlochenwei@hust.edu.cn

X. Tian  
China-EU Institute for Clean and Renewable Energy  
Huazhong University of Science and Technology  
Wuhan, Hubei 430073, China

S. Zhang, Y. Zhang  
School of Materials Science and Engineering & Henan Institute of Advanced Technology  
Zhengzhou University  
Zhengzhou, Henan 450001, China  
E-mail: zhangss124@zzu.edu.cn

Z. Liu, W. Chen  
Hubei Province  
Optics Valley Laboratory  
Hubei 430074, China

W. Chen  
Shenzhen Key Laboratory of Nanobiomechanics  
Shenzhen Institutes of Advanced Technology  
Chinese Academy of Sciences  
Shenzhen, Guangdong 518055, China

 The ORCID identification number(s) for the author(s) of this article can be found under <https://doi.org/10.1002/solr.202200280>.

DOI: 10.1002/solr.202200280

stability of PSCs requires back to fundamental material science and device design. Many works have been reported to reveal the understanding of instinct stability of perovskite material.<sup>[1,3,10,11]</sup>

The structural stability of perovskites with  $\text{ABX}_3$  crystal structure plays a critical role in PSC's stability. The "A" cation represents methylammonium (MA), formamidinium (FA), or cesium (Cs) cation; the "B" cation represents a heavy metal cation, lead, or tin; and the "X" is a halogen: iodide, bromide, chloride, or their combination. In general, the structure stability can be predicted by the Goldschmidt tolerance factor,  $t:t = \frac{R_A + R_X}{\sqrt{2}(R_X + R_B)}$  where  $R_A$ ,  $R_B$ ,  $R_X$  are the atomic radius of the A, B, X ions, respectively.<sup>[12]</sup> Theoretically, t more significant than 1 produces hexagonal and cubic structures, but less than 0.71 can form perovskite. Later, Bartel and coworkers gave a modified tolerance factor,  $\tau:\tau = \frac{R_X}{R_B} - n_A \left( n_A - \frac{R_A/R_B}{\ln(R_A/R_B)} \right)$ , where  $n_A$  is the oxidation state of the A cation.<sup>[13]</sup> Utilizing these two combinations could generally estimate the structural stability for perovskites. According to these two factors, the choices of A, B, and X-site ions are essential for perovskite structure stability. For example, the phase stability of perovskite material can be tuned by the selection of B-site cations and X-sites anions, such as Sn/Pb and I/Br ratios for the structural stability of perovskites. Similarly, selecting an A-site cation with an appropriate size also largely affects perovskite structure stability. To better understand the stability of mixed A-site halide perovskite, we present a function of the Gibbs free energy of mixing ( $\Delta G_{\text{mix}}$ ) of A-site composition at constant pressure and volume:  $\Delta G_{\text{mix}} = \Delta H_{\text{mix}} - T\Delta S_{\text{mix}}$  where  $\Delta H_{\text{mix}}$  is the enthalpy of mixing and  $T\Delta S_{\text{mix}}$  is the entropy of mixing. A-site compositions with  $\Delta G_{\text{mix}} < 0$  form a shared single phase but compositions with  $\Delta G_{\text{mix}} > 0$  prefer to phase segregate and are dependent on temperature. Hence, the suitable choice of A-site cations with low  $\Delta G_{\text{mix}} (<0)$  could lead to a more stable perovskite structure.<sup>[14]</sup> Thus, this function would give the theoretical design for A-site perovskite and an understanding of the stability of A-site cation in PSCs. Finally, perovskite shows strong defect tolerance capability which is different from other semiconductors like silicon. This stems from the unique ionicity and band structure of perovskite material.<sup>[15]</sup> Herein, we will not give more details on this point in this review. More details can be referred to relevant works and reviews.<sup>[3,16–19]</sup> Apart from the instinctive structure stability problem bothering the PSCs, environmental factors, such as moisture, oxygen, heat, light, and electrical biasing, can induce severe degradation of PSCs, leading to adverse effects decay of the device performance. Thus, exploring and evaluating the degradation pathways of perovskites and the degradation mechanisms of PSCs under different environments is very important.

To reveal the degradation mechanisms of PSCs, many characterization techniques have been used. In these characterization techniques, high-resolution electron microscopy (EM) is one of the most used techniques to observe the morphology or structure evolution of the samples. For example, scanning electron microscopy (SEM) is usually used for micro-zone morphology characterization and transmission electron microscopy (TEM) is used for ultrastructure characterization, which can be used to give visualized information for the evolution of PSCs under stress.

In addition, other kinds of microscopies can be used in combination with micromorphology. Energy-dispersive X-Ray (EDX) is a spectroscopy technique that usually acted as a sub-technique of SEM and TEM to determine the distribution and content of the elements in the samples. In addition, Kelvin probe forced microscopy (KPFM) is one of the electrical characterizations in scanning probe microscopy and can map the surface potential or work function of the sample, which can give the electrical changes of the device under ageing.<sup>[20]</sup>

In addition, X-Ray-assisted characterizations are useful tools to observe the crystallography of samples. X-Ray diffraction (XRD) can be used to analyze the crystal structure of bulk film samples using the diffraction effect of X-Ray. X-Ray photoelectron spectroscopy (XPS) is usually used to characterize the surface chemical states change of samples with the photoelectric energy analyzer. Meanwhile, the prevalent characterization technique, grazing incidence wide-angle X-Ray scattering (GIWAXS), can reflect accurately the film on the surface structure information with wide-angle X-Ray scattering, which can give information such as crystal orientation, crystal structure, and crystal morphology.<sup>[21]</sup>

Furthermore, optical spectroscopies are also useful to characterize the degradation of PSCs. Photoluminescence (PL), electroluminescence (EL), light-beam-induced current (LBIC) are the commonly used tools for detecting the photoelectric property of perovskite films and devices. The difference is that PL is a fluorescence spectrum detection for the electronic structure of perovskite material and device, EL is a luminescence spectrum for photoelectric of material and device, and LBIC detects these characteristic parameters through the absorption distance of different laser wavelengths in semiconductors and micro-region photoelectric conversion. As well, other optical spectroscopies, such as UV-visible spectroscopy (UV-vis) utilizing continuous wavelength scanning can be used to analyze the optical properties of samples, and ultraviolet photoelectron spectroscopy (UPS) is usually used to obtain the photoelectron spectrum for the valence electron structure by the ultraviolet light source as the excitation source.<sup>[22]</sup>

As shown in **Figure 1**, XRD, XPS, GIWAXS are mostly used to characterize the composition and crystal structure of perovskite materials,<sup>[23–26]</sup> SEM and TEM are mostly used to visually characterize the microscopic morphology of perovskite films,<sup>[27]</sup> PL, EL, and LBIC are mostly used to characterize the optoelectronic properties of devices.<sup>[3,23,28,29]</sup> These various characterization methods have laid a compacted foundation for investigating

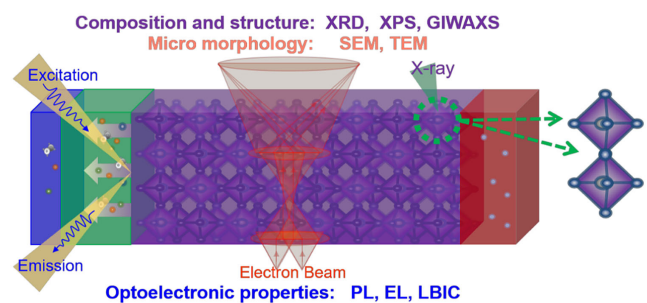


**Figure 1.** Summary schematic of characterization techniques in the research field for perovskite solar cells (PSCs).

the degradation of perovskite materials. Many researchers have used these characterization methods to get a glimpse of the changes in the morphology, crystal structure, and optical properties of the perovskite materials and devices caused by the degradation.<sup>[1,7,30]</sup> However, these traditional characterization methods can only characterize the changes of perovskite materials and devices before and after aged to deduce the degradation mechanism, but lack the direct evidence of intermediate products or changes during the degradation processes, which may miss intermediate degradation stability processes governing devices stability.

In recent years, researchers have devoted themselves to achieving a real-time observation of the degradation process of perovskite materials and devices. In situ characterization techniques for perovskite materials and devices have emerged and made significant progress. In situ characterization techniques enable the huge improvement in observation of dynamical and uniform changes in the crystal structure, morphology, and optoelectronic properties of PSCs, which can reveal the degradation mechanism, which has been put forward and summarized in many works by ex situ characterizations more intuitively, accurately, and dynamically. Thus, these powerful tools become more and more crucial for the understanding of PSCs' stability issues.

This review focuses on the in situ and operando characterizations for observation and measurement of the degradation processes induced by the extrinsic stability stress factors like moisture, heat, light, and electric fields. First, these in situ characterization techniques' exploration and discovery of the PSCs degradation process are systematically summarized and discussed. When exposed to external stimuli, the progress of the degradation of perovskite materials and devices in morphology, crystal structure, and optical properties are demonstrated. Then, we discussed the beam damage issues as well as the corresponding solutions of in situ characterization techniques. At last, this review provides additional suggestions and prospects for the further development and application of in situ characterization technology, which could help better understand the degradation processes of perovskite materials and solve the stability problems that plague the commercialization of PSCs.

## 2. In Situ Characterization of Degradation in Perovskite Solar Cells

Recently, many ex situ characterization results have laid a great foundation for the understanding of PSCs' degradation mechanism triggered by environmental and some realistic operation conditions. Although commonly used ex situ characterizations can offer helpful information about the degradation of perovskite material by characterizing the end products of degradation. The real-time intermediate chemical and structural changes during the degradation under different factors cannot be completely detected by ex situ characterizations, but in situ characterization techniques can achieve this goal. Therefore, in situ characterization is more accurate to trace the degradation process of PSCs under different emulating operating conditions based on ex situ characterization techniques.<sup>[31]</sup>

Since the film morphology, crystallinity, and optoelectronic properties of PSCs govern the performance of PSCs, in situ characterization of these properties is very helpful for the understanding of the degradation processes under the previously discussed external stress factors. First, the micro-morphological changes of perovskite films during degradation can be studied by several in situ image characterizations with high resolution, such as in situ TEM and SEM, which can give the morphological evolution of PSCs for useful information of microstructure changes. Second, in situ X-Ray-assisted spectroscopies can characterize the evolution of the electronic and crystallographic structure of perovskite materials accurately. Last, in situ optoelectronic characterization can obtain the evolution of carrier dynamics inside of PSCs, primarily ion migration-related phase segregation.<sup>[32–35]</sup>

These in situ characterization results are valuable tools to assess the performance and stability of perovskite material films and devices from a typical  $\text{CH}_3\text{NH}_3\text{PbI}_3$  ( $\text{MAPbI}_3$ ) perovskite to FA and/or Cs mixed-cation halide perovskites. Initially, in situ characterization techniques are widely used to systematically study the  $\text{MAPbI}_3$  thermal and humidity stability and present the degradation process. Later, perovskites with better stability based on FA and/or Cs mixed cations are the main research object with in situ characterization techniques. It is found that mixed-cation halide perovskite films and the corresponding devices show improved thermal stability and different ion migration behaviors under bias- and light-induced phase segregation behavior. In this section, we will review the progress on the in situ characterizations and measurements for different perovskite materials and devices under external stress factors (Table 1).

### 2.1. In Situ EM Characterization

EM has been recognized as one of the best tools for studying the microstructure of the materials due to its high-resolution and 3D solid image.<sup>[35]</sup> It has been widely used in the field of PSCs. In situ EM is a valuable technique to dynamically and precisely observe the changes of the surface morphology and microstructure of perovskite materials during their degradation process under different stressing factors.<sup>[36]</sup>

During the operation of PSCs, it is straightforward to cause various reactions due to external stimuli factors and eventually lead to their degradation. To solve the stability problem, it is imperative to thoroughly study perovskite materials' reactions and degradation mechanisms under external conditions. In situ EM technology provides a powerful way to observe the degradation of perovskite, especially beneficial for revealing the degradation mechanism of perovskite under light, heat, and bias.

#### 2.1.1. Heat

The objective structure of perovskite materials is usually formed at 100–150 °C, approaching which structural changes would happen. Furthermore, the decomposition is prone to occur at relatively low temperatures, leading to a sharp decline in performance. Therefore, there is a specific temperature range where the perovskite materials can remain effective and stable. Therefore, exploring the perovskite materials changing with

**Table 1.** A summary of in situ characterizations and measurements of different perovskite films and devices.

In situ Techniques <sup>a)</sup>	Measurement conditions	Perovskite films/devices	Processing	Main findings	Reference
In situ TEM with HAADF imaging	Heat from 50 to 250 °C	FTO/TiO <sub>2</sub> /MAPbI <sub>3</sub> /spiro-OMeTAD/Au	Double-step fabrication: vacuum conversion (sample A), glove box (B) and air conversion (C, with relative humidity ≈50%)—single-step fabrication: glove box (sample B)	The degradation of the samples prepared under different synthesis conditions is different	[37]
In situ TEM with EDX mapping	Heat from 50 to 250 °C	FTO/TiO <sub>2</sub> /MAPbI <sub>3</sub> /spiro-OMeTAD/Au	Double-step fabrication with relative humidity ≈50%	Iodine migrates first at a low temperature, and lead migrates in the same direction after further heating	[37]
In situ TEM	Heat at 85 °C	MAPbI <sub>3</sub>	N/D	MAPbI <sub>3</sub> is degraded layer by layer to generate a stacked triangular/tetragonal structure that retains the crystal orientation	[40]
In situ TEM with SAED images	Heat at 85 °C	MAPbI <sub>3</sub>	N/D	MAPbI <sub>3</sub> with a tetragonal configuration convert into PbI <sub>2</sub> with a triangular configuration	[40]
In situ HRTEM	Heat from 25 to 170 °C	MAPbI <sub>3</sub>	N/D	Triangular PbI <sub>2</sub> was precipitated from the amorphous MAPbI <sub>3</sub> layer through the asymmetric intermediate state	[41]
In situ HRTEM	Heat to 135 °C	MAPbI <sub>3</sub>	N/D	Thermal degradation of perovskite is usually the inverse process of perovskite film growth	[45]
In situ TEM	Heat to 170 °C	Cs/ FA/MA	N/D	Maintain thermal stability below 150 °C	[46]
In situ TEM	Apply +6 V voltage to HTL side	MAPbI <sub>3</sub>	N/D	Bias triggered the migration of iodide to the positive HTL	[34]
In situ HAADF-STEM, BFTEM, and SAD	Apply a forward bias of +1 V	MAPbI <sub>3</sub>	N/D	A large number of Oxygen atoms in TiO <sub>2</sub> migrated into MAPbI <sub>3</sub> , resulting in the amorphization of MAPbI <sub>3</sub> and the formation of PbI <sub>2</sub>	[47]
In situ HAADF-STEM, BFTEM, and SAD	Remove the forward bias, store in the dark, apply a reverse bias of +1 V	MAPbI <sub>3</sub>	N/D	Oxygen ions escaped from MAPbI <sub>3</sub>	[47]
In situ TEM with SAED	Apply a forward bias of +1 V	(FAPbI <sub>3</sub> ) <sub>x</sub> (MAPbBr <sub>3</sub> ) <sub>1-x</sub>	Double-step fabrication	Bias-induced perovskite amorphous	[31]
In situ SEM	Under illumination	MAPbI <sub>3</sub>	N/D	The light caused the structure to break down into dispersed particles	[48]
In situ grazing incidence X-ray diffraction (GIXRD)	Heat from 50 to 300 °C	FAPbI <sub>3</sub>	N/D	Presented main four stages during annealing and perovskite degraded into PbI <sub>2</sub> at a higher temperature compared with MAPbI <sub>3</sub>	[54]
In situ grazing incidence wide-angle X-ray scattering (GIWAXS),	N/D	FA <sub>0.83</sub> MA <sub>0.17</sub> Pb(I <sub>0.83</sub> Br <sub>0.17</sub> ) <sub>3</sub>	Spin-coating	Found three main phases-formation stages	[55]
In situ XRD	Heat 144/150 °C in the air	Cs <sub>0.17</sub> FA <sub>0.83</sub> Pb(I <sub>0.83</sub> Br <sub>0.17</sub> ) <sub>3</sub>	Spin-coating	Maintained crystallographic texture of perovskite crystallites largely	[56]
In situ XRD	Heat 144/150 °C in the air	Cs <sub>0.05</sub> (MA <sub>0.17</sub> FA <sub>0.83</sub> ) <sub>0.95</sub> Pb(I <sub>0.83</sub> Br <sub>0.17</sub> ) <sub>3</sub>	Spin-coating	Observed two degradation stages: first stage with faster degradation of MA <sup>+</sup> and the second stage with degradation of FA <sup>+</sup> at a higher temperature	[56]
In situ XRD	80% Humidity	MAPbI <sub>3</sub>	Spin-coating	Observed intermediate monohydrate phase and volume expansion	[42]

**Table 1.** Continued.

In situ Techniques <sup>a)</sup>	Measurement conditions	Perovskite films/devices	Processing	Main findings	Reference
In situ GISANS	58%/73%/93%/96 RH	MAPbI <sub>3</sub>	Spin-coating	Formation of monohydrate at 73% RH and dihydrate at 93% and 96% RH, leading to volume expansion	[57]
In situ GIWAX	80%/85% RH under illumination	MAPbI <sub>3</sub>	Spin-coating	Formation of hydrate phase and increasing iodide ions mobility	[58]
In situ pXRD	65%/90% RH with/without illumination	FTO/TiO <sub>2</sub> /MAPbI <sub>3</sub> /spiro-OMeTAD/Au	Spin-coating	Three decomposition stages during the degradation process, leading significant devices performance loss; PbOH occurred with illumination- and moisture-assisted ion migration	[43]
In situ XRD	6 h at the light in vacuum/air	MAPbI <sub>3</sub>	Spin-coating	Faster degradation in the air than in vacuum and light was the trigger of fast degradation	[62]
In situ XRD	Under illumination in ambient condition	MAPbI <sub>3</sub>	Spin-coating	Decomposition from MAPbI <sub>3</sub> to PbI <sub>2</sub>	[63]
In situ XRD	Under white light illumination	MAPb(I <sub>0.4</sub> Br <sub>0.6</sub> ) <sub>3</sub>	Spin-coating	Significant peak broadening resulting from phase segregation	[67]
In situ XRD	Under white light illumination	FACsPb(I <sub>0.4</sub> Br <sub>0.6</sub> ) <sub>3</sub>	Spin-coating	Slight peak broadening resulting from FACs suppressing of phase segregation	[67]
In situ XPS	under X-Ray irradiation at the low dose beamline	FAPbI <sub>3</sub> ) <sub>0.85</sub> (MAPbBr <sub>3</sub> ) <sub>0.15</sub>	Spin-coating	Photoinduced ion migration leads to the decline of device performance	[68]
In situ LBIC	50% RH	MAPbI <sub>3</sub>	Spin-coating	Formation of hydrate and the humidity intruded from the edge of the devices to the center	[71]
In situ KPFM	Heat from 30 to 80 °C	MAPbI <sub>3</sub>	Spin-coating	Contact potential difference decreased with temperature increase and the evolution of carrier migration-induced degradation	[72]
In situ AFM	Heat from 30 to 80 °C under illumination	MAPbI <sub>3</sub>	Spin-coating	Average photocurrent diminishes with temperature increasing	[72]
In situ PL	Electric field: 22 × 10 <sup>4</sup> V m <sup>-1</sup>	MAPbI <sub>3-x</sub> Cl <sub>x</sub>	Spin-coating	Electric bias caused iodine vacancies migration and enhanced non-radiative recombination	[73]
In situ PL	Under illumination	MAPbI <sub>3</sub>	Spin-coating	Formation dynamics of photoinduced phase segregation and visualized iodide-rich domains in surface	[76]
In situ PL	Under laser illumination, 10–100 mW cm <sup>-2</sup> , 457 nm	(MA)Pb(Br <sub>x</sub> I <sub>1-x</sub> ) <sub>3</sub>	Spin-coating	PL peak showed redshift and tails resulting from phase segregation	[75]
In situ PL	Under light soaking	MAPbI <sub>3</sub>	Spin-coating	Ion migration under light leads to reduce charge-carrier separation and increase recombination	[28]
In situ PL	Under laser illumination	FACsPb(I <sub>0.8</sub> Br <sub>0.2</sub> ) <sub>3</sub> FACsPb(I <sub>0.5</sub> Br <sub>0.5</sub> ) <sub>3</sub> FACsPb(I <sub>0.4</sub> Br <sub>0.6</sub> ) <sub>3</sub>	Spin-coating	Found an additional PL peak from higher Br concentration (Br ≥ 0.5) and formation of I-rich phase	[67]
In situ PL	Under 1 sun continuous illumination in air	Cs <sub>0.05</sub> (FA <sub>0.87</sub> MA <sub>0.13</sub> ) <sub>0.95</sub> Pb(I <sub>0.87</sub> Br <sub>0.13</sub> ) <sub>3</sub>	Spin-coating	PL peak redshift related to phase segregation	[77]

<sup>a)</sup>Abbreviations: (N/D: none data).

temperature and the thermal response process of PSCs is crucial for developing PSC devices.

Ducati and colleagues used in situ TEM experiments to obtain the thermal response of four unencapsulated PSC

samples with the same device structure of fluorine-doped tin oxide (FTO)/TiO<sub>2</sub>/MAPbI<sub>3</sub>/spiro-OMeTAD/Au but based on different manufacturing ways. In their experiment, samples A (in vacuum), B (in the glove box), and C (in air, 50% relative

humidity (RH)) were fabricated by a two-step approach, and sample D (in the glove box) was manufactured by a one-step method. High-angle circular dark-field (HAADF) imaging was used to record the degradation process of the four samples at different heating stages, as the cross-sectional images shown in Figure 2a. After being heated to 150 °C, the perovskite layer of device C was the first to undergo noticeable changes, as the temperature increased to 225 °C, the perovskite layer in samples A, B, and D began to degrade. During degradation, small particles were formed at the interface, and as the temperature further rose, the tiny particles began to migrate and coalesce. Figure 2b shows the HAADF image of sample C after heating at different temperatures and the corresponding EDX element diagrams of iodine and lead. When sample C was heated, the diffusion of heavy elements in the hole transport layer (HTL) could be seen in the HAADF signals. The EDX mapping confirmed the first iodine migration at a low temperature (50 °C), and lead was observed

to migrate in the same direction after further heating to a higher temperature (175 °C).<sup>[37]</sup> Their in situ EM experiments were based on micro-heaters on the sample holders. Their results clearly reveal the behavior of perovskite under heating, which is very helpful for the understanding of heat-induced degradation of perovskite. It is the first time to observe the degradation of perovskite by in situ EM. Through the in situ observation of the device cross section, the morphological changes of perovskite devices under thermal stress were breakthrough and intuitive characterized in this work. This is a pioneering work to reveal the principle of perovskite degradation by in situ EM. Indeed, EM is very useful for materials structure study, however, the influence of the electron beam on the long scanning process and the influence of the sample preparation process should not be ignored. Similarly, through in situ TEM imaging, Yang and coworkers observed the microscopic phenomenon of perovskite decomposition at 50–60 °C under illumination. They also

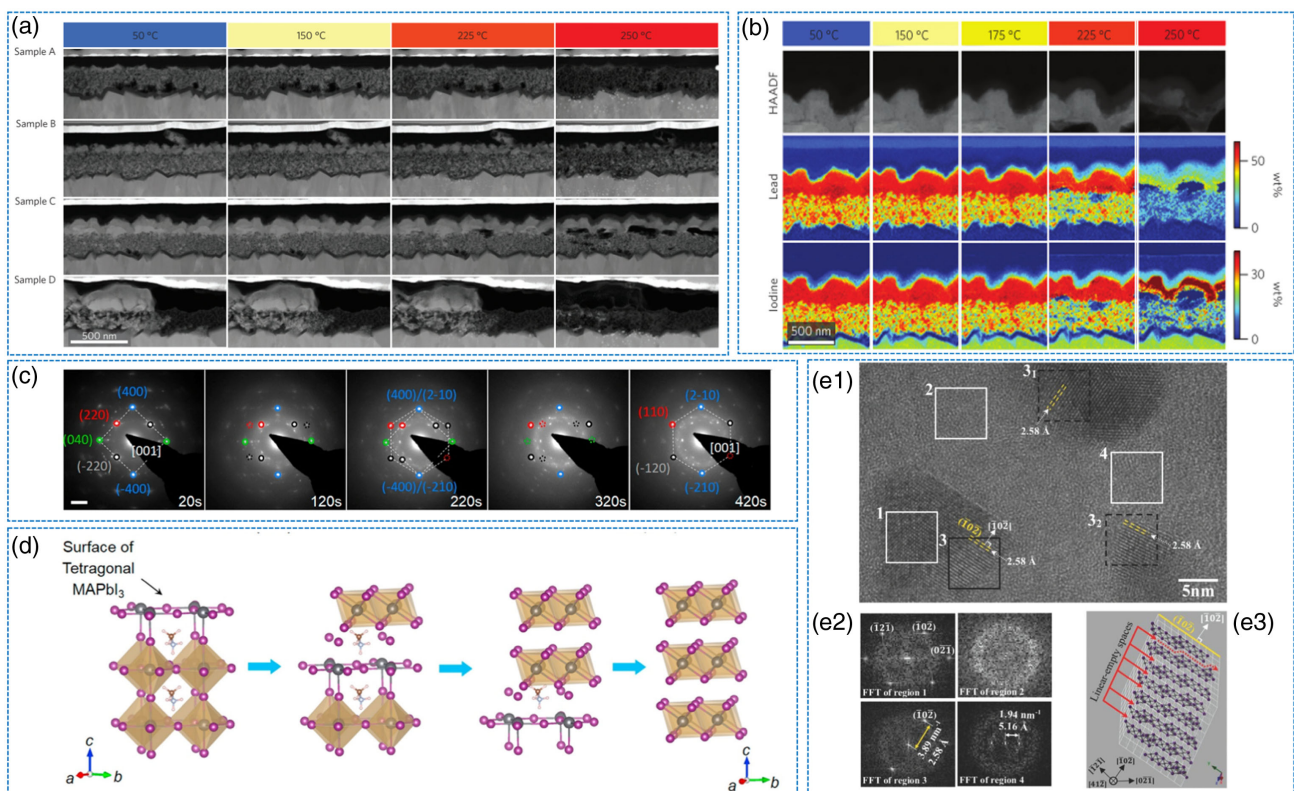


**Figure 2.** In situ electron microscopy (EM) observation of perovskite under heat. a) Cross-sectional scanning transmission electron microscope high-angle circular dark-field (STEM-HAADF) images of four samples in different manufacturing ways (A, vacuum; B, glove box; C, air; D, single step) at different stages of heating with 50 °C acting as the base temperature for the transmission electron microscope (TEM) analysis. In the HAADF image, the brightness is directly proportional to the average atomic number and thickness. b) The HAADF images and Energy-dispersive X-Ray (EDX) elemental maps for iodine and lead of sample C after different steps of heating. The heating steps performed at 175 °C are kept for 30 min, and those performed at temperatures above 200 °C are kept for 15 min due to the faster sample dynamics. The same scale bar applies to all panels. Reproduced with permission.<sup>[37]</sup> Copyright 2016, Macmillan. c) In situ monitoring of the structure evolution of MAPbI<sub>3</sub> in reciprocal space. d) The tetragonal MAPbI<sub>3</sub> surface retains the crystal orientation and makes transition layer by layer to the PbI<sub>2</sub> layer; with the degradation process, the bottom layer is exposed to a new surface layer. Reproduced with permission.<sup>[40]</sup> Copyright 2017, Elsevier. e1) Enlarged view of high-resolution TEM (HRTEM) image after heating at 170 °C for 7 min and 15 s; the FFT and atomic configuration simulation are along the [412] perfect triangle PbI<sub>2</sub>. e2) Region 1:[412] FFTs with axial triangular PbI<sub>2</sub> grains, region 2: amorphous diffraction patterns, region 3: asymmetric (102) diffraction points obtained by the boundary of triangular PbI<sub>2</sub> grains and amorphous phase, and region 4: the early stage of triangular PbI<sub>2</sub> precipitation. Areas 31 and 32 are the same as areas 3. e3) Thin plate of a simulated cross-section of PbI<sub>2</sub> crystal along [412] perfect triangle. Reproduced with permission.<sup>[41]</sup> Copyright 2018, Wiley-VCH.

found that heating would cause element migration and lead to perovskite degradation. Moreover, they demonstrated that the degradation of the perovskite would be affected by defects. After heating, the degradation around the damaged part of the beam was more apparent, and the entire perovskite layer was also significantly degraded.<sup>[38]</sup> Their results were consistent with those of Ducati et al., which further confirm that thermal degradation of perovskite is largely affected by its existing defects. In addition, Aguiar and coworkers also observed the redistribution and migration of lead ions occurring in perovskite beds at high temperatures using *in situ* TEM.<sup>[39]</sup> These studies have fully characterized the degradation of perovskite at a macro level, further detailed degradation process at the atomic level is still not presented, which is encouraged in future study.

With an environmental gas cell, Fan and coworkers used *in situ* TEM to observe the atomic changes as the structural evolution of the perovskite hybrid during the heating process.<sup>[40]</sup> They characterized the evolution process from tetragonal MAPbI<sub>3</sub> to trigonal PbI<sub>2</sub> by the reciprocal space *in situ* selected area electron diffraction (SAED) images. As shown in Figure 2c, at the beginning 20 s, the initial tetragonal lattice phase was observed; with heating at 85 °C, the evolution of the crystal structure began, and the original tetragonal pattern gradually evolved into a triangular pattern of PbI<sub>2</sub> from 20 to 220 s; at 420 s, the tetragonal MAPbI<sub>3</sub> was finally transformed into a standard trigonal PbI<sub>2</sub>. In addition, they revealed the layer-by-layer degradation path starting from the crystal surface for the first time. As shown in Figure 2d, MAPbI<sub>3</sub> is degraded layer by layer to generate a stacked triangular/tetragonal structure that retains the crystal orientation.<sup>[40]</sup> The layer-by-layer degradation mechanism is well studied in this work. Meanwhile, the authors improved the configuration of *in situ* EM and realized *in situ* study of thermal degradation of perovskite by the use of an environmental gas cell, which is also a very significant work and can broaden the ideas for the development of *in situ* EM in the future. Kim and his colleagues reported similar results through *in situ* HRTEM and fast fourier transform (FFT) imaging. As shown in Figure 2e1,e2, the detailed precipitation processes of triangular PbI<sub>2</sub> particles were observed during the thermal degradation. It was confirmed that the triangular PbI<sub>2</sub> was precipitated from the amorphous MAPbI<sub>3</sub> layer through the asymmetric intermediate state, rather than from the crystallized MAPbI<sub>3</sub> layer.<sup>[41]</sup> The asymmetric intermediate state and its stacking can form a 3D linear channel that allows elements to pass through, providing a path for the decomposition of perovskite.<sup>[42–44]</sup> Through *in situ* HRTEM images and corresponding FFT, Wang and coworkers also observed the transformation of MAPbI<sub>3</sub> into amorphous phase and the precipitation of triangular PbI<sub>2</sub> grains under the stress of heat, proving once again that thermal degradation of perovskite is related to its growth path, as usually the inverse process of perovskite film growth, as shown in Figure 2e3.<sup>[45]</sup>

As well known, due to the relatively high interaction between FAPbI<sub>3</sub>-based perovskites and lead-halide octahedrons, FAPbI<sub>3</sub>-based perovskites have better thermal stability than MAPbI<sub>3</sub>-based perovskites. Seo and coworkers observed MA-based PSCs' performance and FAMACs-based PSCs under constant heating and found that the two perovskites have different degradation mechanisms through *in situ* TEM. During the heating process, MA-based PSCs showed rapid degradation in the

perovskite film, while FAMACs-based PSCs remained stable at 130 °C, and began to degrade at 150 °C, and when heated to 170 °C, the degradation of FAMACs-based PSCs is more serious.<sup>[46]</sup> This is because the methanaminium iodide (MAI) is highly volatile and MA-based PSC is prone to intense thermal decomposition during heating, but the FA cation, compared with the MA cation, is less volatile and shows stronger hydrogen bond interaction, which makes FA-based PSC have higher thermal stability as shown in the *in situ* TEM heating contrast experiment.

From the previous reports, we can conclude that the use of FACs-based perovskites can effectively improve thermal stability compared with MA PSCs. The cation radius of FA<sup>+</sup> is larger than that of MA<sup>+</sup>, leading to the enhancement of the combination between FA and PbI<sub>6</sub> cation so that FAPbI<sub>3</sub> with an even more proper bandgap of ≈1.48 eV shows better thermal stability than MAPbI<sub>3</sub>. And its performance in other aspects will be continued in the following section.

### 2.1.2. Electrical Bias

The extra voltage can also cause degradation of the PSCs. Jeangros and coworkers conducted *in situ* TEM experiments to reveal the bias-induced degradation mechanism of perovskite materials. They applied a voltage of +6 V on the HTL side of the cell and found that iodide ions migrated to the positively biased charge transport layer after a few minutes, PbI<sub>2</sub> nanoparticles appeared on the interface of MAPbI<sub>3</sub>/HTL, and the MAPbI<sub>3</sub> layer shrank slightly. When the voltage was continued to be applied, PbI<sub>2</sub> nanoparticles continued to be generated and the MAPbI<sub>3</sub> layer further shrank, as shown in Figure 3a. Thus, it was believed that the bias triggered the migration of iodide to the positive HTL and accelerated the volatilization of I and organic matter (mainly at the positively biased MAPbI<sub>3</sub> interface), which resulted in the nucleation and voiding of PbI<sub>2</sub> nanoparticles and thereby reduced the device performance.<sup>[34]</sup> This work first realized the *in situ* EM observation of perovskite degradation under electric bias, which presented the migration of iodide under electric bias and deepened understanding of the bias-induced degradation mechanism of perovskite. At the same time, it proposed an *in situ* EM device for *in situ* observation under electric bias. In this article, the extra degradation caused by the process of preparing samples with a focused ion beam (FIB) is described. Their *in situ* experiments EM were achieved through contacting the sample with the microelectromechanical system chip. But this will introduce a lot of joule heat and test results will be affected.<sup>[47]</sup>

Jung and coworkers used an *in situ* electric-biased TEM to study the structural changes of n-i-p MAPbI<sub>3</sub>-based solar cells with TiO<sub>2</sub> as the ETL caused by the bias. Through HAADF-scanning transmission electron microscope (HAADF-STEM) image, bright-field (BF)-TEM image, and selected area diffraction (SAD) image of the same area inside the MAPbI<sub>3</sub> single crystal grain, an interesting phenomenon was observed, as shown in Figure 3b. Under forward bias, a large number of O atoms in TiO<sub>2</sub> migrated into MAPbI<sub>3</sub>, resulting in the amorphization of MAPbI<sub>3</sub> and the formation of PbI<sub>2</sub>. When the bias voltage was removed, and the sample was stored in the dark, the reversible oxygen migration exhibited, returning from MAPbI<sub>3</sub> to TiO<sub>2</sub>,

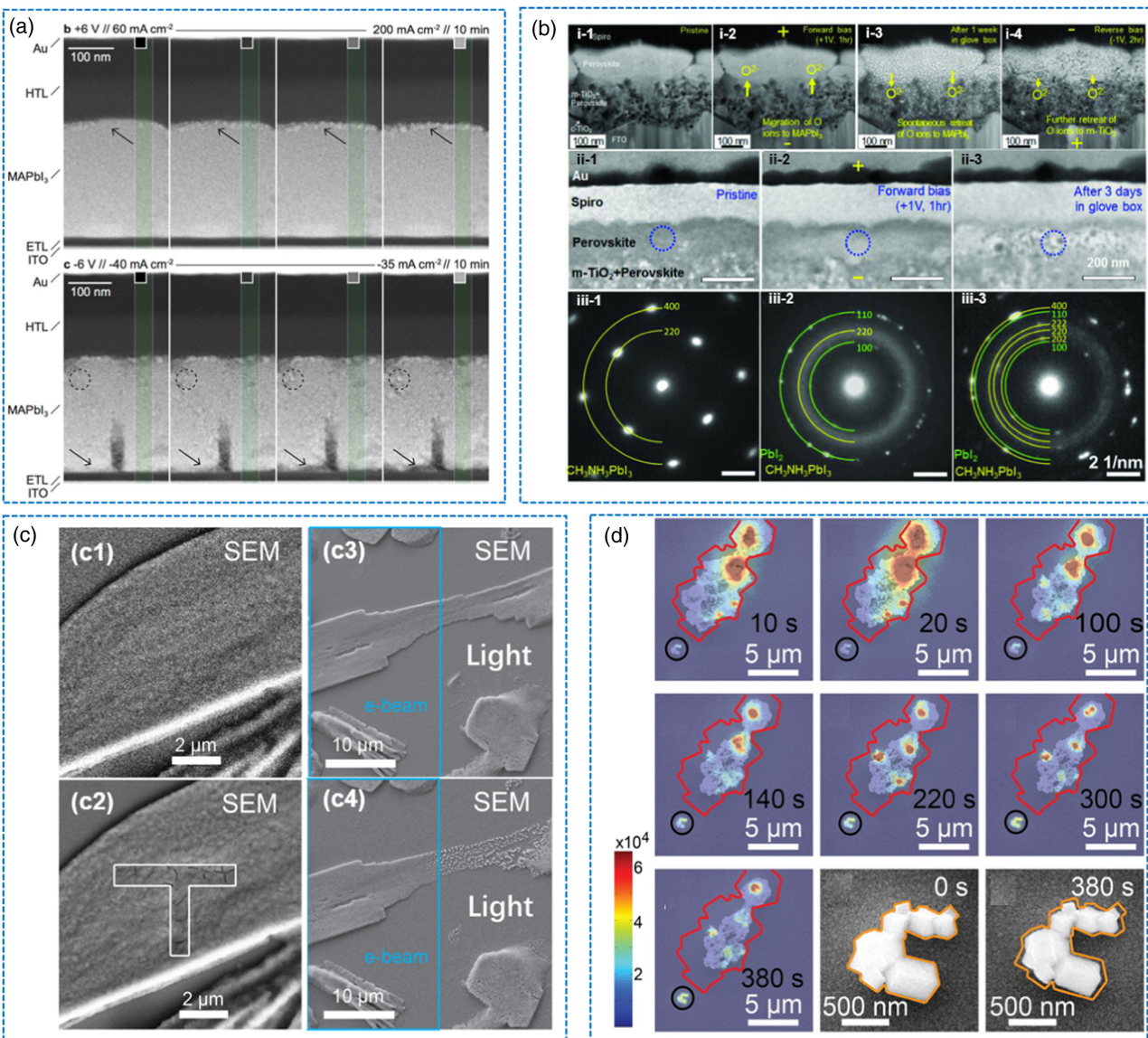


**Figure 3.** a) HAADF images acquired when biasing for 10 min at +6 V (up) and -6 V (down), which result in the current density increased from 60 to 200 mA cm<sup>-2</sup> and decreasing from -35 to -40 mA cm<sup>-2</sup>, respectively, along with corresponding HAADF intensity profiles integrated over the width of the shaded area. Arrows and circles highlight the formation of nanoparticles and the consequent shrinkage of the MAPbI<sub>3</sub> phase during biasing, while arrowheads display a polarity-dependent increase in HAADF intensity at the position of the charge transport layers. Reproduced with permission.<sup>[34]</sup> Copyright 2016, American Chemical Society. b) Series of i) HAADF-STEM, ii) bright-field TEM (BFTEM), and iii) selected area diffraction (SAD) of MAPbI<sub>3</sub> solar cell devices (1) of the pristine conditions, (2) after applying a forward bias of +1 V, (3) after the storage for 1 week in an Ar glove box, and (4) after applying a reverse bias of -1 V. Note that SADs were taken from the same selected area of MAPbI<sub>3</sub> (blue dotted circle) in the BFTEMs, where the yellow rings represent MAPbI<sub>3</sub> and the green rings represent PbI<sub>2</sub>. Reproduced with permission.<sup>[47]</sup> Copyright 2018, Wiley-VCH. c) Structural changes induced by e-beam treatment: c1) scanning electron microscopy (SEM) micrograph with the minimum electron beam dose acquired on the original perovskite film; c2) SEM micrograph acquired on the identical area after drawing the "T" pattern highlighted with solid lines (a guide to the eye); c3) SEM micrograph acquired before laser illumination (the left half of the structure highlighted with a cyan square is subjected to e-beam scanning (86 pA, 10 kV) for 5 min); c4) SEM micrograph on the same area in panels f and g after laser illumination. d) Structural and photoluminescence (PL) evolution of two cuboid clusters upon degradation. SEM and PL images are overlapped on the identical area at 10, 20, 100, 140, 220, 300, and 380 s, respectively. Compared with the original shape outlined with the orange solid lines, the dimensions of the cluster shrank almost evenly at each direction for about 40 nm. Reproduced with permission.<sup>[48]</sup> Copyright 2016, American Chemical Society.

and the crystallinity of MAPbI<sub>3</sub> was partially restored. After applying a reverse bias on the partially recovered device, it was found that more oxygen ions escaped from MAPbI<sub>3</sub>, and

partially recovered the performance degradation caused by the long-term forward bias.<sup>[47]</sup> The ions in the electron transport layer will migrate into MAPbI<sub>3</sub> under the bias voltage, causing

MAPbI<sub>3</sub> to be amorphic and precipitating PbI<sub>2</sub>. This change is partially reversible. When the bias voltage is removed, or the bias voltage in the opposite direction is applied, the ions from MAPbI<sub>3</sub> escape. In situ EM experiments achieved through contacting the sample with the microelectromechanical system chip will introduce a lot of joule heat, which will affect the test results.<sup>[47]</sup> The introduction of an electrical bias holder for in situ characterization can isolate the effects of an electrical bias from other factors that affect the long-term stability of perovskite in a device configuration. This further promoted the development of in situ EM. This work also confirms the oxygen ion migration within the device under electric bias and investigates the reversible degradation of perovskite devices under electric bias for the first time, which can be partially recovered under inert gas environments and reverse bias.

Kim and coworkers used in situ HRTEM with SAED analysis to observe the degradation performance of FAMA mixed-cation perovskite materials under bias in real time.<sup>[31]</sup> They found that bias can induce ion migration and lead to perovskite amorphous. Under the continuous 1 V forward bias, the lattice fringes of the perovskite crystal gradually disappeared, and wholly disappeared after 300 s, and a clear amorphous ring appeared in the SAED pattern. Furthermore, they showed through detailed analysis that the amorphous form only occurs in the perovskite phase.

Under biasing stressing factor, the mixed FAMA-based perovskite materials do not show apparent advantages for inhibiting the ion migration compared with MAPbI<sub>3</sub> perovskite materials. Therefore, more designed in situ EM studies of these mixed FAMA perovskite materials about ion migration are needed.

### 2.1.3. Light Illumination

As a solar cell converts solar energy into electrical energy, it naturally needs to work under light illumination. However, PSCs have specific instability problems under such conditions. Therefore, the research on the light-induced degradation of perovskite materials needs to be improved. Yuan and his colleagues used in situ TEM experiments to study the degradation of perovskite films induced by electron beam and light, respectively. Figure 3c1 shows the SEM micrograph with the minimum electron beam dose acquired on perovskite film, and Figure 3c2 is obtained in the same area after drawing the T-shaped pattern with solid lines (pointing to the eye). It can be observed that obvious cracks with a width of about 20 nm exist on the surface of the perovskite. It is the structural degradation caused by the electron beam. Figure 3c3,c4 are SEM images before and after electron beam scanning (area within the blue frame, scanning for 5 min) and illumination (area on the right, illumination for a few seconds), respectively. Minor structural deformations appeared on the surface of the perovskite under the action of the electron beam, while light caused the structure to break down into dispersed particles. This work further characterizes the light-induced degradation of perovskite, clearly showing the morphological changes of perovskite under light soaking.

In situ EM can also be combined with other in situ technologies to more clearly and comprehensively observe the degradation of perovskite. Yuan and coworkers combined in situ SEM with PL for the first time to observe the electron beam-induced

morphological changes and optical properties of the perovskite film in real time. The simultaneous reduction of PL intensity and shape size caused by degradation was observed, as shown in Figure 3d.<sup>[48]</sup> Under the illumination of the electron beam, the PL intensity of the two clusters decreases with the increase of illumination time, and the size of the clusters also decreases with the increase of illumination time. The change rate of the larger clusters is faster than that of the smaller clusters. The perovskite film will degrade under the irradiation of the electron beam, which is heterogeneous. They point out that high-energy electrons can cause extra damage to the material, and to avoid this, a 10 kV acceleration voltage can be used in the experiment. The vacuum will remove the volatile gases produced after degradation, resulting in irreversible degradation. Simultaneously, this work subtly utilized these two in situ technologies to more accurately illustrate the degradation process of perovskite under external stress, which is of great significance to further construct the degradation mechanism of perovskite in detail.

To date, utilizing in situ EM to study light-induced degradation is rarely reported. As the potential stable FACs mixed-cation perovskite materials, light-induced ion migration, especially halide ion migration, would lead to phase segregation. Therefore, in situ EM could make the phase segregation visual and in-real time, which would be essential to study the complete light-induced degradation processes.

In situ EM technology has made EM research develop from static to dynamic. Through in situ EM technology, the dynamic sensing information of the sample to the environment is captured, and the microstructure changes of the material are more directly correlated with external signals, which can provide a deeper understanding of the PSC degradation mechanism. As a very practical high-end characterization technology, in situ EM can directly observe the microstructure evolution process of the sample under heat, bias, and light at the atomic level with extremely high resolution. However, EM characterizations still have some shortcomings for perovskite degradation study. First, EM has certain requirements for the sample. For example, the cross-sectional electron microscope measurement requires the device to be cut into slice samples for scanning. The cutting surface is required to be smooth and flat, and the device structure cannot be damaged. FIB preparation is one of the commonly used slice sample preparation techniques, which is usually by focusing the ion beam into a very small ion beam to bombard the surface of the material to achieve exfoliation, deposition, implantation, cutting, and modification of the material, causing slight damage to the material. Recently, a cryo-focused ion beam (cryo-FIB) has been developed to reduce damage during slice sample preparation.<sup>[49]</sup> Second, high-resolution images need to be obtained under a high-energy electron beam, which could cause electron beam damage to the material, affecting the accuracy of the observation results. This problem can be lessened by controlling the dose of the electron beam, normally using 10 kV acceleration voltage can effectively impair this damage. Third, the vacuum environment could remove volatile products, owning a negative impact for studying the degradation process, thus this is still a major technical difficulty to overcome. Moreover, although the in situ EM has achieved remarkable development in a short period, there are still some difficulties to be overcome, including vacuum extraction of volatile products due to the

vacuum degree requirements of the EM, which is impossible to carry out water and oxygen. Meanwhile, the water vapor will be ionized under the irradiation of the electron beam, dispersing the energy of the electron beam, resulting in blurred images, and it will react with the high-temperature tungsten filament, reducing the lifetime of filament. As technology advances, it may be possible to solve this problem one day by adding extra chambers and so on.<sup>[50]</sup>

## 2.2. In Situ X-Ray-Assisted Characterization

X-Ray-assisted characterization techniques are useful tools to study the crystal structure, chemical composition, and morphology of perovskite materials and devices. Since X-rays inherit a typical advantage that with suitable wavelength can penetrate most atmospheres and apparatus itself especially compared with electron beam characterizations, the X-Ray source can be easily employed for in situ characterization to monitor the evolution of perovskite material and film under moisture, heat stress, light, and electronic bias conditions applied in apparatus. Thus, in situ X-Ray-assisted techniques have been widely used to monitor the chemical, structural, and morphological changes of the perovskite films and devices ranging from the perovskite formation to degradation, especially for the dynamic changing process for perovskite.

### 2.2.1. Heat

Early studies utilizing ex situ characterizations on perovskite films and devices revealed the changes of perovskite film morphology, crystal structure, and phase after annealing. At higher temperatures, many studies have verified the perovskite layer would do decompose by ex situ tools. However, it's necessary to comprehensively understand the effect of thermal stress on PSCs degradation. In situ X-Ray-assisted characterization tools can efficiently monitor the crystallization development during the fabrication process of perovskite films, especially in the annealing step.

Stone and coworkers utilized in situ X-Ray-assisted characterization and in situ X-Ray diffraction and revealed the transformation from precursor to MAPbI<sub>3</sub> phase.<sup>[51]</sup> Figure 4a shows the waterfall composite plots of in situ XRD and representative XRD scans of perovskite film fabricated by one-step spin-coating when in situ annealing was at 100 °C for 5, 30, and 70 min, respectively. It is noticed that three stages showed up in the annealing step. The first 5 min drying stage corresponded to the precursor phase's crystallization, with the characteristic diffraction peaks at  $q = 0.85, 0.90$ , and  $1.1 \text{ \AA}^{-1}$ . From 5 to 20 min, no perovskite phase ( $q = 1.0 \text{ \AA}^{-1}$ ) showed up, thus this stage was referred to as the latent stage. However, from 20 to 70 min, a continued loss of precursor phase tally with the growth of the perovskite phase. This phase transformation of MAPbI<sub>3</sub> film during annealing was able to be observed and three stages could be tracked dynamically and continuously, which is difficult to implement in ex situ X-Ray techniques. This work confirmed that in situ X-Ray diffraction could be a workable technique to trace the perovskite film's phase transformation during the annealing process. In addition to the observation of the phase transformation

of perovskite samples, more investigations about the crystal structure transformation of perovskite material or even devices under thermal stressing operation can also be studied by in situ X-Ray spectroscopy. Kim and coworkers studied the thermal degradation progresses within MAPbI<sub>3</sub> when a higher temperature was applied on perovskite film more systematically, based on in situ X-Ray spectroscopy of 2D GIXAXS, HR-XPS, and near edge X-ray absorption fine structure (NEXAFS) in the surface of MAPbI<sub>3</sub>.<sup>[52]</sup> As shown in Figure 4b,c, the phase of MAPbI<sub>3</sub> transformed from tetragonal phase into cubic phase and then started thermal degradation at 100 °C, with the intermediate phase appearing ( $q = 0.55 \text{ \AA}^{-1}$ ). After that, the perovskite MAPbI<sub>3</sub> decomposed into PbI<sub>2</sub>, CH<sub>3</sub>I, and NH<sub>3</sub>. The film heated at 130 °C appeared a strong peak at  $q = 0.9 \text{ \AA}^{-1}$ , which was assigned as the (001) plane of PbI<sub>2</sub>. Thus, the decomposition of perovskite into PbI<sub>2</sub> via the intermediates was verified. From Figure 4d, the surface changed into a region rich in Pb and I but poor in MA above 100 °C, which confirmed that the film decomposition started from the surface to the bulk, leaving only the PbI<sub>2</sub> on the surface (after the evaporation of CH<sub>3</sub>I and NH<sub>3</sub>). Thus, this in situ tool presents the advantage of tracing intermediate degradation products and decomposition paths.

Moreover, Tan and coworkers utilized in situ GIWAX to investigate the structure and film morphologies of MAPbI<sub>3-x</sub>Cl<sub>x</sub>.<sup>[53]</sup> As shown in Figure 4e, the crystalline precursor of MAPbI<sub>3-x</sub>Cl<sub>x</sub> was detected at peak  $q = 11 \text{ nm}^{-1}$  after 3 min at 30 °C. When annealed at 80 °C for 50 min, a scattering ring showed up at  $q = 10 \text{ nm}^{-1}$ , which indicated the transition from the crystalline precursor to polycrystalline perovskite. Figure 4e revealed the structure transition was completed at the point of 60 min at 90 °C. When the temperature was raised to 100 °C, at the point of 70 min, the perovskite film started to degrade and proceed to the final point of 120 min, with PbI<sub>2</sub> as a perovskite degradation product. Their work is effective to verify the structure transition during annealing and thermal degradation. Their work was consistent with the results from the aforementioned two works and this in situ X-Ray-assisted technique indeed could track the whole crystalline structure transformation process for MA-based perovskite material from annealing to degradation under heat stress, which is very helpful for the understanding of perovskite degradation under heating stressing.

To improve the heat stability of MA perovskite, Meng and coworkers considered using FA<sup>+</sup> cation as the substitution of MA<sup>+</sup> cation. First, they utilized in situ GIXRD to investigate FAPbI<sub>3</sub> perovskite films during the annealing process. They presented four stages during heat from 50 to 300 °C. Initially, PbI<sub>2</sub>, formamidinium iodide (FAI), and  $\alpha/\delta$ -FAPbI<sub>3</sub> originated complex diffraction patterns with superposition of diffraction peaks at stage I. At stage II, the peak of PbI<sub>2</sub> disappeared and films showed both  $\alpha$  and  $\delta$ -FAPbI<sub>3</sub> phases with FAI diffusing as the temperature increased to 100 °C. With temperature elevating to 150 °C, the pure  $\alpha$ -FAPbI<sub>3</sub> showed up indicating the total conversion of non-perovskite phases and depletion of FAI at stage III as temperature elevated to 150 °C. Then, they found as the temperature further increased to 300 °C, the perovskite degraded into PbI<sub>2</sub>, the higher temperature for FAPbI<sub>3</sub> perovskite began to degrade into PbI<sub>2</sub> at the stage IV.<sup>[54]</sup> This work is helpful to understand the FAPbI<sub>3</sub> perovskite structure transition under thermal stressing and beneficial to further demonstrate the

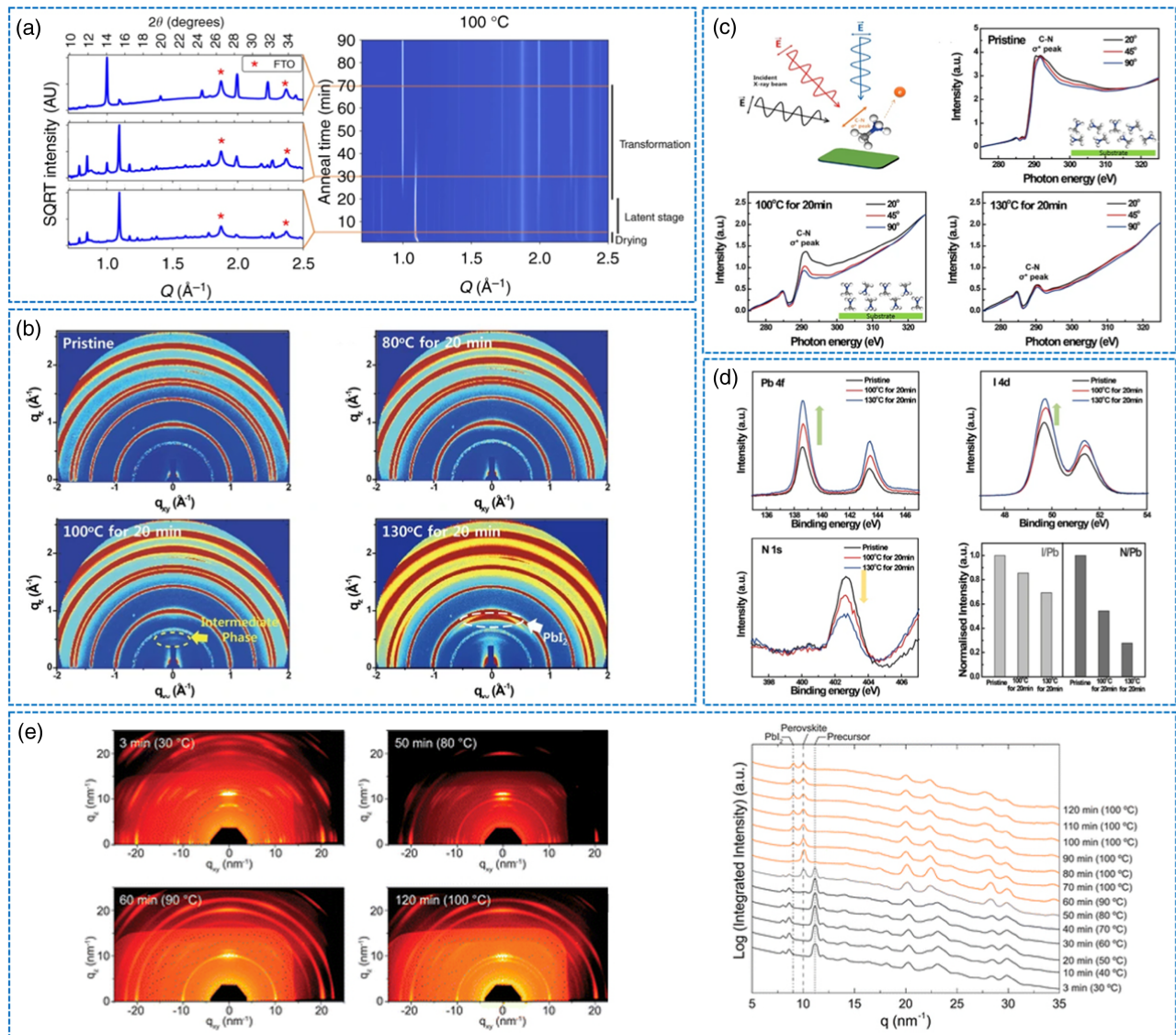


**Figure 4.** a) In situ X-Ray diffraction of perovskite annealing at 100 °C (XRD scans shown are a 5 min of the end of drying, 30 min during the transformation, and 70 min near the end of the transformation) and left side of Waterfall composite plot: each horizontal slice corresponds to an XRD pattern at a certain time. Reproduced with permission.<sup>[51]</sup> Copyright 2018, Springer Nature. b) In situ 2D grazing incidence wide-angle X-Ray diffraction (GIWAXD) patterns of MAPbI<sub>3</sub> perovskite films determined under different thermal conditions: pristine MAPbI<sub>3</sub>, MAPbI<sub>3</sub> exposed to 80 °C for 20 min, 100 °C for 20 min, and 130 °C for 20 min, respectively. Reproduced with permission.<sup>[52]</sup> Copyright 2017, Springer Nature. c) Schematic diagram of NEXAFS measurements. Angle-resolved carbon K-edge in situ NEXAFS spectroscopy of MAPbI<sub>3</sub> perovskite film before and after heating at 100 °C for 20 min and 130 °C for 20 min. Reproduced with permission.<sup>[52]</sup> Copyright 2017, Springer Nature. d) In situ high-resolution X-Ray photoelectron spectroscopy (HR-XPS) spectra determined under different temperature conditions for Pb 4f (recorded with excitation energy of 200 eV), I 4d (200 eV), N 1s (500 eV) of MAPbI<sub>3</sub>, and changes in the N/Pb and I/Pb ratios as a function of heat exposure. Reproduced with permission.<sup>[52]</sup> Copyright 2017, Springer Nature. e) The 2D grazing incidence wide-angle X-Ray scattering (GIWAXS) profiles for MAPbI<sub>3</sub> perovskite films annealed in nitrogen for 3, 50, 60, and 120 min, together with azimuthally integrated intensity plots. Reproduced with permission.<sup>[53]</sup> Copyright 2014, American Chemical Society.

thermal degradation mechanism. This final thermal degradation product was similar to that for MA-based perovskite but the phase transformations differed from MA-based perovskite. These useful results can be easily obtained by utilizing in situ X-Ray-assisted characterization. Meanwhile, it is recognized that the Cs<sup>+</sup> cation replacing MA<sup>+</sup> cation replacing a part of iodide anions with Br<sup>-</sup> and Cl<sup>-</sup> could improve heat stability. First of all,

Qin and coworkers utilized in situ GIWAXS to trace mixed perovskite FA<sub>0.83</sub>MA<sub>0.17</sub>Pb(I<sub>0.83</sub>Br<sub>0.17</sub>)<sub>3</sub> crystal formation during annealing. They found three main phase-formation stages: 1) precursor solution, 2) hexagonal δ-phase, and 3) complex phases including hexagonal polytypes and intermediate phases.<sup>[55]</sup> These complex phase transformations were consistent with the previous FA-based perovskite results. Their work confirms

the phase transformation of FA-based perovskite, which indicates the mixed perovskite indeed could enhance the thermal stability. Then, Tan and coworkers utilized *in situ* XRD compared with the thermal stability of mixed-cation organic-inorganic lead-halide perovskite  $\text{Cs}_{0.17}\text{FA}_{0.83}\text{Pb}(\text{I}_{0.83}\text{Br}_{0.17})_3$  and  $\text{Cs}_{0.05}(\text{MA}_{0.17}\text{FA}_{0.83})_{0.95}\text{Pb}(\text{I}_{0.83}\text{Br}_{0.17})_3$  to verify this thermal stability enhancement from the replacement of  $\text{FA}^+$  and  $\text{Cs}^+$  cations and observed the first stage with a faster degradation rate mainly involving  $\text{MA}^+$  at relatively low temperature ( $T < 150^\circ\text{C}$ ) and second stage mainly involving  $\text{FA}^+$  at higher temperature for  $\text{Cs}_{0.05}(\text{MA}_{0.17}\text{FA}_{0.83})_{0.95}\text{Pb}(\text{I}_{0.83}\text{Br}_{0.17})_3$  perovskite film. At  $144^\circ\text{C}$  annealing,  $\text{Cs}_{0.17}\text{FA}_{0.83}\text{Pb}(\text{I}_{0.83}\text{Br}_{0.17})_3$  maintained the crystallographic texture of perovskite crystallites primarily during decomposition reaction.<sup>[56]</sup> This enhancement of thermal stability for mixed perovskite is traceable from the *in situ* results about phase transformation involved in *in situ* annealing from MA-based perovskite to FA-based perovskite. This *in situ* structure transformation under different temperatures effectively proves the better thermal stability for FA-based perovskite material. These *in situ* results consistently affirm the better thermal tolerance of FA/Cs-based perovskite implying the effective thermal stability improvement of mixed-halide perovskite.

Thus, the phase transition and structural change processes during annealing- and heat-induced degradation at higher temperatures can be dynamically observed in the usage of *in situ* X-Ray characterizations. This further deepens the understanding of the heat-induced degradation of PSCs. Based on these *in situ* characterization results of  $\text{MAPbI}_3$  film under temperature elevating, it is easily found  $\text{MAPbI}_3$  thermal unstable and degraded into  $\text{PbI}_2$  causing irreversible degradation. Substituting  $\text{MA}^+$  cation with  $\text{FA}^+$ ,  $\text{Cs}^+$  cation to form mixed-cation perovskite is effective to improve thermal stability and enhance crystallinity and structural stability.

### 2.2.2. Humidity

It is well known that the halide PSCs are sensitive to humid ambient conditions. *In situ* X-Ray tools are useful to track the changes in crystal structure and products of humidity-induced degradation, especially to verify the appearance of mono/dihydrate.

Li and coworkers utilized *in situ* XRD to indicate the formation of monohydrate with  $\text{MAPbI}_3$  film exposed to 80% humidity.<sup>[42]</sup> As shown in Figure 5a, at the initial stage of 0 to 5.5 h, no significant amount of the hydrate phase was observed, with only the  $\text{MAPbI}_3$  structure with (110) plane. With prolonging the exposure to 80% humidity, the monohydrate  $\text{MAPbI}_3 \cdot \text{H}_2\text{O}$  with space group P21/m was formed, corresponding to the (101) and (100) crystal plane. Figure 5b plots the X-Ray diffraction pattern versus time, and the transformation process is visualized. This transformation of perovskite to the monohydrate could lead to a volume expansion, which may be the trigger of the hysteresis in *I-V* behavior. Their finding of hydrate phase from *in situ* results affirms the existence of intermediate hydrate product under high humidity. Moreover, this volume expansion from lattice expansion could also be presented in the *in situ* XRD results. To further figure out the reversibility of humidity-induced transformation, the film subsequently was dried in  $\text{N}_2$  gas after exposure

to humidity, following the hydration-dehydration cycle. As shown in Figure 5b, even the film was exposed to 80% humidity for 65 h, after the flushing of  $\text{N}_2$  gas, the monohydrate would disappear, but the intensity of perovskite could not return to its initial intensity possibly due to only a portion of monohydrate phase converted back into perovskite phase. Their findings implied the monohydrate as a key intermediate transition phase for humidity-induced degradation.

To track the kinetics of changes more carefully in the structure of perovskite film as the ingress of different contents of moisture, Schlipf and coworkers utilized *in situ* grazing incident small-angle neutron scattering (GISAXS) and heavy water ( $\text{D}_2\text{O}$ ) as deuterium to detect the amorphous phase. Figure 5c1 showed the representative 2D neutron scattering patterns of a dry and hydrate film, respectively, as well as an intense specular peak caused by the direct reflective beam. The left of the specular peak, the Yoneda peak, represented an increased diffuse signal. It moved to the right (the higher angels) during hydration, which indicated the  $\text{MAPbI}_3$  film incorporated a large portion of water molecules by forming the hydrate phases accumulated between the grains and the non-regions of domains, but not directly incorporated into the perovskite crystal structure. As shown in Figure 5c2, the Yoneda peak showed no significant change for  $\leq 58\%$  RH, indicating no hydrates were formed. The small changes in the Yoneda peak revealed the formation of monohydrate for 73% RH and dihydrate for 93% and 96% RH. Similarly, the formation of mono/dihydrate would expand the volume of crystal at high RH; at low RH, no significant expansion was observed. Thus, the results directly confirmed that the content of humidity plays an important role in structural changes for PSCs, which is important for the understanding of humidity-induced degradation.<sup>[57]</sup>

In addition to the structural changes, the humidity could induce ion migration, which also would lead to the degradation in perovskite-based devices. Fransishyn and coworkers operated an *in situ* GIWAX to study  $\text{MAPbI}_3$  PSCs at 80% and 85% RH under illumination, revealing that the hydrate phase is not the only important degradation path for perovskite devices, while the increasing mobility of iodide leads to the corrosion of the metallic at the top contact. From Figure 5d1 and d2, we can see the intensity of (110) peak ( $q = 1.01 \text{ \AA}^{-1}$ ) dropped within 1.6 h but no significant hydrate phase appeared. At 85% RH within 6.5 h, the loss of intensity of perovskite (110) peak was bigger and no new phase appeared. This result was high with the previous finding that high RH would allure the hydrate formation. However, the hysteresis in the *I-V* curve indicated the ion migration in PSCs, especially for that with the silver electrode, compared with the gold-based devices. No hydrate and decomposition products appeared, which may be coincident with the results in Figure 5d3. When applied halogen lamp to increase the device's temperature, the photothermal annealing would suppress the formation of hydrate phases and crystalline decomposition products.<sup>[58]</sup> It indicates *in situ* techniques can be useful tools to demonstrate the diminishment of PSCs' performance from phase changes and structural changes and help to reveal the humidity-induced degradation mechanism.

Similarly, Chen and coworkers studied  $\text{MAPbI}_3$ -based perovskite devices utilized *in situ* powder-XRD (PXRD).<sup>[43]</sup> As shown in Figure 5e, the devices of FTO/TiO<sub>2</sub>/MAPbI<sub>3</sub>/spiro-OMeTAD/

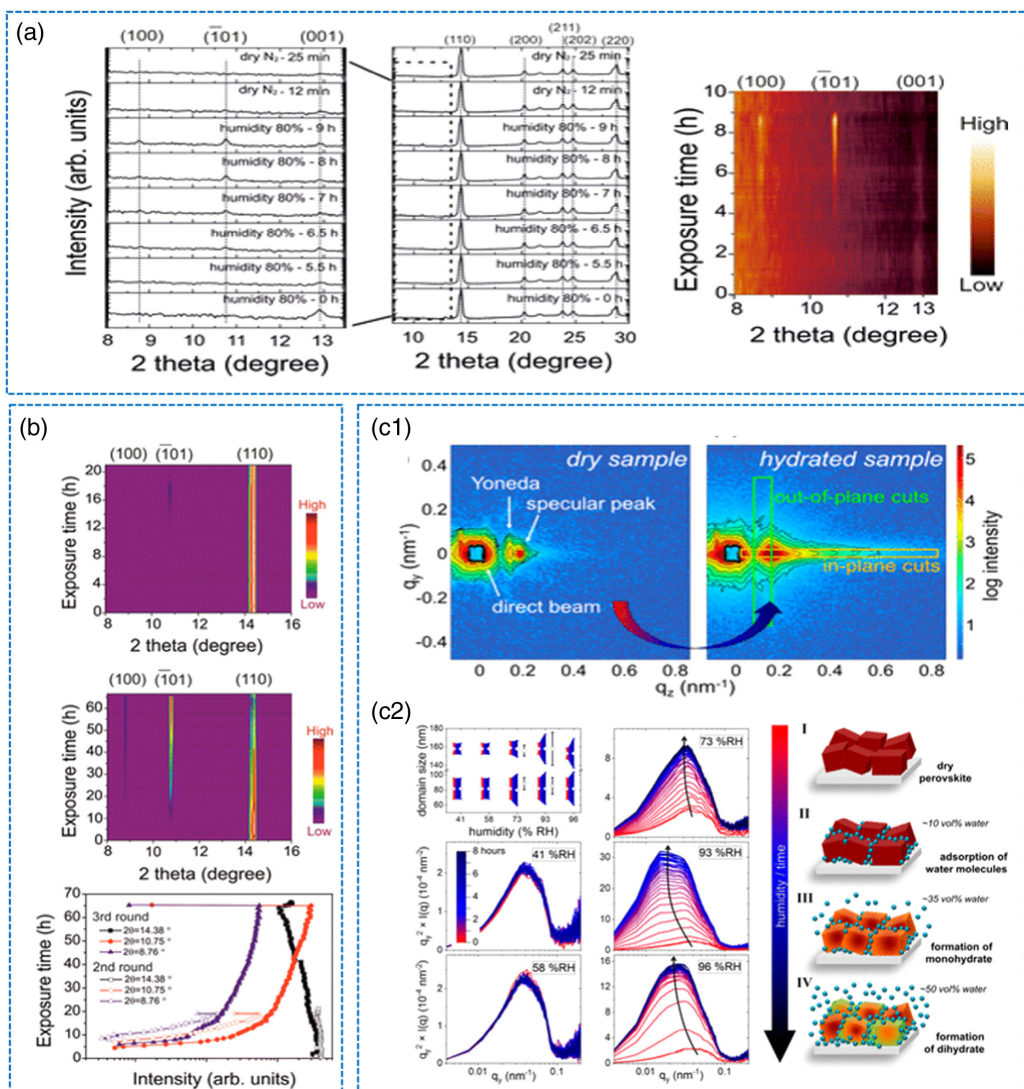


**Figure 5.** a) Time-resolved in situ XRD of a MAPbI<sub>3</sub> film during the first hydration–dehydration round and the corresponding contour plot showing changes in XRD peak intensity during the first hydration–dehydration cycle. Reproduced with permission.<sup>[42]</sup> Copyright 2016, American Chemical Society. b) Contour plots of the time-resolved peak intensity of XRD data at the second and the third hydration–dehydration cycles, as well as the integrated intensities of the Bragg reflections as a function of exposure time. Reproduced with permission.<sup>[42]</sup> Copyright 2016, American Chemical Society. c1) The 2D grazing-incidence small-angle neutron scattering (GISANS) data with a logarithmic color code and integration time of 1 h. Direct beam, specular peak, and Yoneda peak are marked in the left image, while cut positions are shown in the right image. It is obvious that the incorporation of D<sub>2</sub>O leads to an increased scattering signal and the Yoneda peak shifts toward the specular peak. c2) Domain sizes with Gaussian distribution around a mean value (symbol) with size distribution (standard deviation depicted as bars) under various humidity levels for dry (red), hydrated (blue) and dehydrated (black) films. At a humidity of 73% RH, the domain sizes become more distributed. As a guide-to-the-eye, the standard deviation is interpolated and the area is filled with a color gradient resembling the time of the exposure. Kratky-style plots for the samples exposed to various humidity levels from 41% RH to 96% RH. Reproduced with permission.<sup>[57]</sup> Copyright 2018, American Chemical Society. d1) and d2) Azimuthally integrated GIWAXS patterns for an indium tin oxide (ITO)/ZnO/MAPbI<sub>3</sub>/P3HT/Ag PSCs after exposure to a nitrogen atmosphere with the RH of 80% and 85%, with I-V curves acquired at 1 min intervals. Reproduced with permission.<sup>[58]</sup> Copyright 2018, American Chemical Society. d3) GIWAXS pattern of an ITO/ZnO/ MAPbI<sub>3</sub>/P3HT/ Ag device exposed to a nitrogen atmosphere with RH ≈ 90%. The device was left in the dark and illuminated for brief periods with either a halogen or light emitting diode (LED) light source, as noted in the figure. While illuminated, the X-Ray exposures were limited to 0.5 s and the scattering intensities were corrected to compensate. Reproduced with permission.<sup>[58]</sup> Copyright 2018, American Chemical Society. e) Contour plots of in situ X-Ray diffraction measurement and the corresponding cell performance along with time evolution at 65% RH and 25 °C under nitrogen environment. Reproduced with permission.<sup>[43]</sup> Copyright 2017, American Chemical Society.

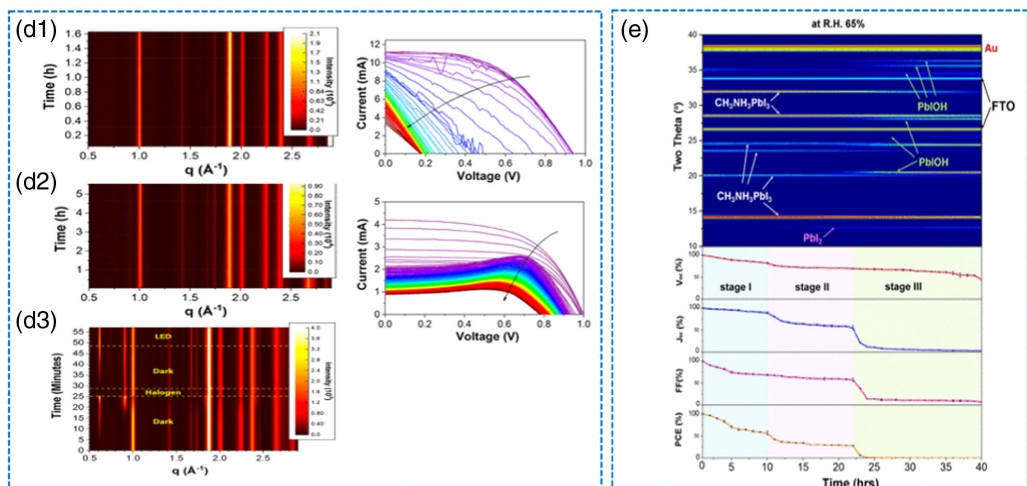


Figure 5. Continued.

Au at 65% and 90% RH showed three decomposition stages during the degradation process induced by humidity, according to the performance changes of PSCs. The first stage involved the formation of hydration and it led to the loss of fill factor. The second stage is related to the decomposition from MAPbI<sub>3</sub> to PbI<sub>2</sub> with the significant loss of the device performances. At the last stage, peaks coincident with PbIOH occurred, which were attributed to the combination of illumination- and moisture-assisted ion migration. PbIOH only appeared when taking spiro-OMeTAD as HTL. Thus, the option of HTL is considered to play an important role in humidity-induced degradation progress.

Although FAPbI<sub>3</sub> owns distinguished thermal stability compared with MAPbI<sub>3</sub>, its sensitivity to moisture would cause structural instability in the presence of humidity. Adding Cs<sup>+</sup> cation into FAPbI<sub>3</sub> perovskite could improve the humidity stability due to the balance of tolerance factor.<sup>[59]</sup> Hu and coworkers utilized in situ XRD and EDX to study the Cs cation impact to perovskite FA<sub>0.83</sub>MA<sub>0.17</sub>Pb(I<sub>0.83</sub>Br<sub>0.17</sub>)<sub>3</sub> at 75% RH and they found Cs<sup>+</sup> cations were incorporated into the multiple-cation perovskite to contract the lattice and stabilize the photoactive perovskite phase under moisture condition.<sup>[60]</sup> In addition to the intrinsic regulation of the perovskite composition, encapsulation can be a useful tool to protect the perovskite from moisture and oxygen.<sup>[61]</sup>

These in situ X-Ray-assisted tools are useful to characterize the structural changes during the humidity-induced degradation process and under different contents of water conditions. The in situ results from low RH and high RH are apparently different, indicating the possibility of reversible humidity-induced degradation under the former case. Moreover, in situ X-Ray-assisted tools could track the intermediate product, monohydrate and dihydrate appearance and even irreversible decomposition product, PbI<sub>2</sub> from perovskite material, and so on.

### 2.2.3. Light Illumination

In situ X-Ray techniques can also offer a better understanding of the light-induced degradation of PSCs. Tang and coworkers

utilized in situ XRD to dynamically present the structural changes induced by light.<sup>[62]</sup> In Figure 6a1–a4, the diffraction peak of MAPbI<sub>3</sub> vanished, while the peak of PbI<sub>2</sub> ( $\theta = 39.5^\circ$ ) and metal Pb ( $\theta = 31.4^\circ$  and  $36.3^\circ$ ) appeared and increased rapidly only after 6 h of exposure to light in a vacuum. This revealed that MAPbI<sub>3</sub> easily decomposed into PbI<sub>2</sub> and metal Pb only after 6 h. Furthermore, the peaks of perovskite diminished faster in the air than in a vacuum. Thus, the faster decomposition exposure to light in the air compared to dark/air indicated that light was the trigger of the fast decomposition of perovskite. Moreover, the peak of PbI<sub>2</sub> soon reached its maximum after 2 h and then decreased slowly, which indicated the photolysis of PbI<sub>2</sub>. Under air conditions, the photolysis of PbI<sub>2</sub> would further cause lead salt as a degradation product. Similarly, Senocrate and coworkers observed the decomposition process from MAPbI<sub>3</sub> to PbI<sub>2</sub> under illumination with oxygen by using in situ XRD.<sup>[63]</sup> Therefore, the light in ambient conditions would be a worthy accelerated ageing factor in the stability study of PSCs. This work suggested that in situ X-Ray-assisted characterizations are effectively to study the light-induced degradation process.

Recently, mixed-cation metal halide PSCs have been demonstrated to own excellent PCE and durability against damp heat.<sup>[64–66]</sup> However, the photoinduced ion migration is another cause for degradation of PSCs and it will lead to the phase segregation of PSCs. Sutter-Fella and coworkers utilized in situ XRD to invest the halide segregation of MA- and FA-based perovskite film, as shown in Figure 6b. Figure 6b showed the (100) peaks of MAPb(I<sub>0.4</sub>Br<sub>0.6</sub>)<sub>3</sub> and FACsPb(I<sub>0.4</sub>Br<sub>0.6</sub>)<sub>3</sub> film, where the peak of MA film showed a significant peak broadening and peak asymmetry but the peak of FACs film showed only a slight peak broadening. The new peak of the MA-film was related to the new I-rich phase with different lattice parameters. The changes were attributed to halide segregation. Compared with MA-based PSCs, FACs-based ones cannot relax strain accumulated during the halide demixing, suppressing the phase segregation.<sup>[67]</sup> The photoinduced ion migrations usually increase the defect concentration, leading to the decrease in performance of devices, but no significant structural change could be found in the perovskite

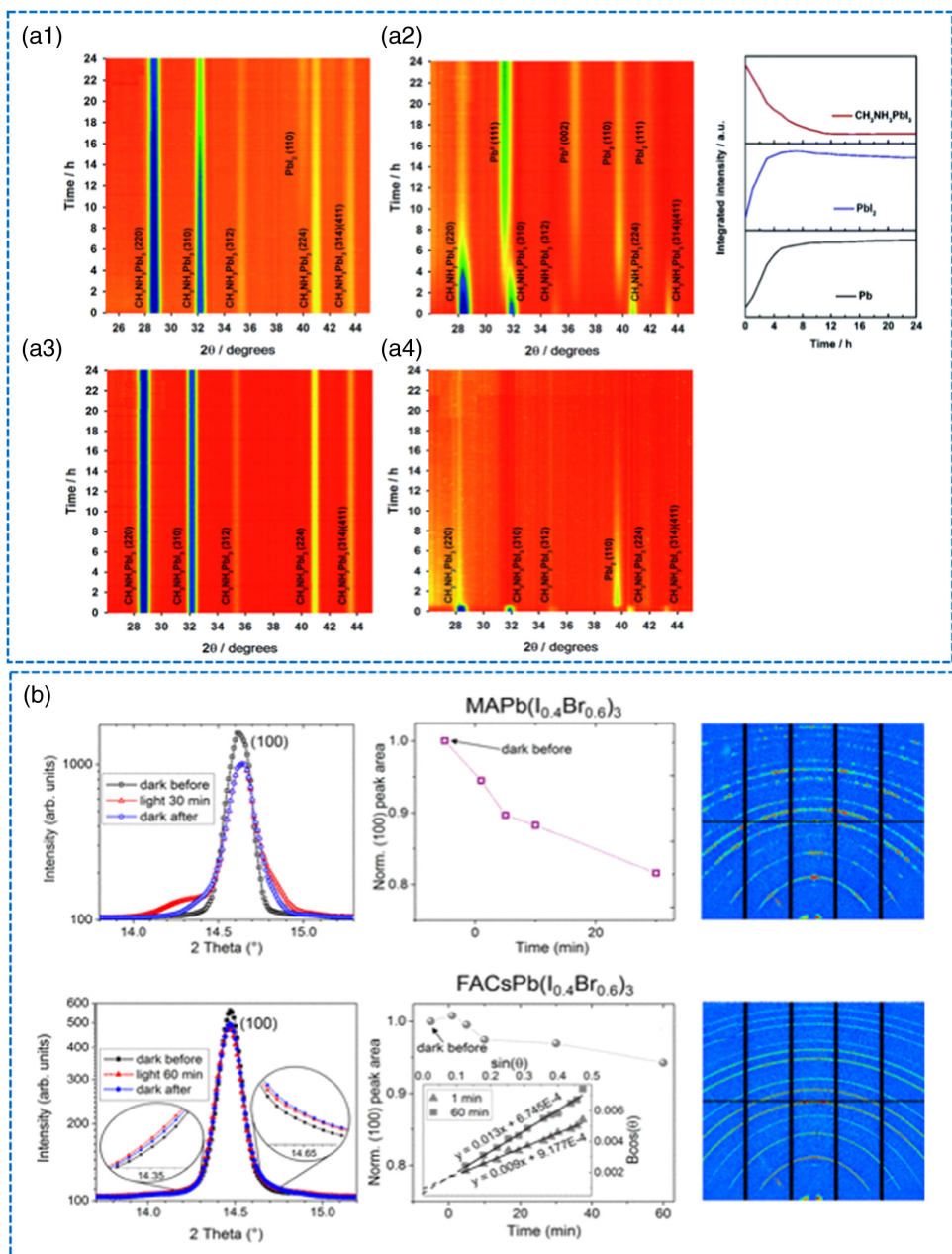


**Figure 6.** a1,a2) In situ XRD of MAPbI<sub>3</sub> films at 350 K under a1) vacuum/dark and a2) vacuum/light, and integrated intensity calculated from in situ XRD patterns of MAPbI<sub>3</sub> films at 350 K under vacuum/light. a3,a4) In situ XRD spectra for MAPbI<sub>3</sub> films under air at 350 K without or with light illumination. Reproduced with permission.<sup>[62]</sup> Copyright 2016, Royal Society of Chemistry. b) In situ X-Ray diffraction MAPb(I<sub>0.4</sub>Br<sub>0.6</sub>)<sub>3</sub> and FAPb(I<sub>0.4</sub>Br<sub>0.6</sub>)<sub>3</sub> samples at different states: before illumination, during illumination, and after relaxation in the dark; and the normalized peak area under illumination over time. Reproduced with permission.<sup>[67]</sup> Copyright 2018, Royal Society of Chemistry. c) Time evolution of the I 4d spectra measured with a photon energy of 120 eV and Br 3d spectra measured with a photon energy of 139 eV at different states: before, during, and after laser illumination at 515 nm with a power of 0.52 mW. The black horizontal lines indicate where the laser was switched on (5 min) and off (35 min). Only one spin doublet is seen in each case, indicating that no formation of new I and Br specimens is observed in the solid state. Comparison of the intensities of Pb 5d, I 4d, and Br 3d versus time is obtained by fitting the individual spectra, where the intensities are normalized to the intensity before laser illumination for each core level and linear fit lines are included during and after laser illumination. Reproduced with permission.<sup>[68]</sup> Copyright 2017, Royal Society of Chemistry.

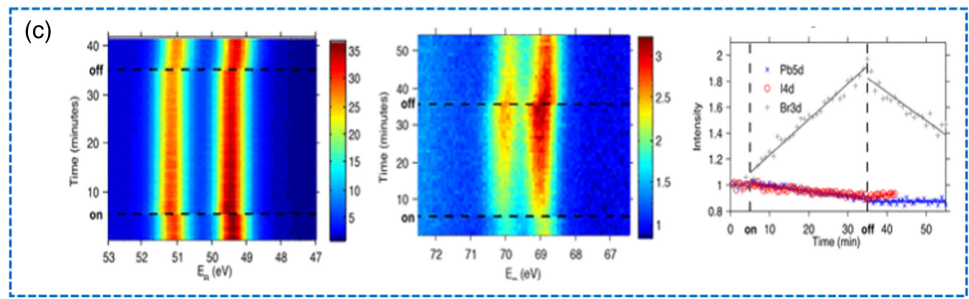


Figure 6. Continued.

layer. Thus, it is not easy to directly observe by *in situ* XRD. *In situ* XPS could be a valuable tool for studying the photoinduced phase segregation of mixed-halide PSCs. Cappel and coworkers utilized *in situ* XPS to observe the migration of bromide ions to the surface and the decrease of concentration of  $\text{Pb}^{2+}$  and iodide at the surface, as shown in Figure 6c.<sup>[68]</sup> It is easily concluded FA and/or Cs replacing MA as the A-site could increase grain size, and change the equilibrium defect concentrations or lattice stiffness, which effectively inhibit the phase segregation compared with  $\text{MAPb}(\text{Br}_x\text{I}_{1-x})_3$  perovskite film.

The photoinduced ion migration may be related to the decline in the performance of perovskite devices. The photoinduced phase segregation is normally characterized by photoluminescence spectra, which will be introduced in the following section. Utilizing *in situ* X-Ray-assisted characterizations is still challenging to investigate the photoinduced ion migration problems.

There still exist some limitations for these advanced *in situ* X-Ray-assisted characterizations. Utilizing *in situ* X-Ray-assisted characterizations to investigate the ion migration induced by different stressing factors within devices and impact on device performance is limited because the most popular *in situ* X-Ray-assisted characterizations prefer to show the crystal structure changes and degradation products appearance precisely rather than directly present the ion migration.

### 2.3. In Situ Optoelectronic Characterization

*In situ* optoelectronic characterization is an important tool to study the degradation in PSCs. Especially, *in situ* LBIC, PL, and EL are typical *in situ* optoelectronic tools. They could provide beneficial results of the evolution of the carrier dynamics process and ion migration of PSCs under moisture, heat, light, and electrical bias. Thus, they are meant to better understand the degradation mechanism in PSCs and improve the stability of PSCs. Both *in situ* EM and X-Ray techniques can characterize the heat/moisture/light/bias-induced ion migration dynamic degradation process in perovskite devices, but the process always needs to be verified with other means, such as *in situ* EM combining with EDX, and *in situ* X-Ray combining with *I*-*V* curve. However, the *in situ* optoelectronic technique could directly characterize the evolution of carrier dynamics and ions movements during the degradation process induced by the aforementioned factors. In all, these *in situ* optoelectronic characterizations are widely used techniques to directly investigate the carrier

dynamics and recombination kinetics as well as the internal electrochemical potential for free charge carriers within complete devices, the single perovskite absorber layer, or even semiconductor layers with transport layers with intuition and vivid *in situ* results.<sup>[69,70]</sup>

*In situ* LBIC mapping can be applied in PSCs to provide intuitive photocurrent imagine information of the carrier migration responding to the changes under applied stresses. Song and coworkers first carried out *in situ* LBIC to investigate the perovskite degradation process in humidity conditions. Before their work, few LBIC tools were applied to PSCs. As shown in Figure 7a, the external quantum efficiency (EQE) maps present four distinct stages during which the devices were exposed in 50% RH humidity. The first stage showed that the EQE of PSCs increased slightly and reached the peak after exposure for a few minutes. This slight increase was considered the water passivation for the recombination center between the spiro-OMeTAD and perovskite layer, which reduces surface trap states and better carrier extraction. In this stage, the EQE of the entire area was not a constant but with defective areas. The second stage showed that EQE dropped uniformly. This decrease could be related to the doping states and reduced hole collection efficiency. As well, a large number of contributed defects could also attribute to the decrease, like the one at the left of the image. In the third stage, the EQE showed a dramatic drop. As seen from the image, it can be easily concluded that degradation started from the top and progressed downward, which revealed the humidity intruded from the edges of the devices toward the center. Moreover, this dramatic drop coincided with the formation of hydrate phases, which was verified by the XRD result. The last stage surprisingly showed a temporal increase at some locations in PSCs. The high EQE at some spots in the image showed a larger photocurrent during the degradation process, which might be caused by the disproportionation and phase separation to produce anhydrous perovskite particles and materials with poor photoactivity as perovskite hydrate or  $\text{PbI}_2$ .<sup>[71]</sup> This lively *in situ* LBIC mapping tool can thoroughly present the dynamic degradation process, which can help to recognize the ingress direction and away from water and other stressing factors during degradation. But the identification of degradation products and intermediate products is lacking. Therefore, it needs assistance from other characterization tools.

*In situ* KPFM is another useful tool applied in PSCs to offer the direct results of morphology and electrical properties associated with the devices' performance. KPFM can provide

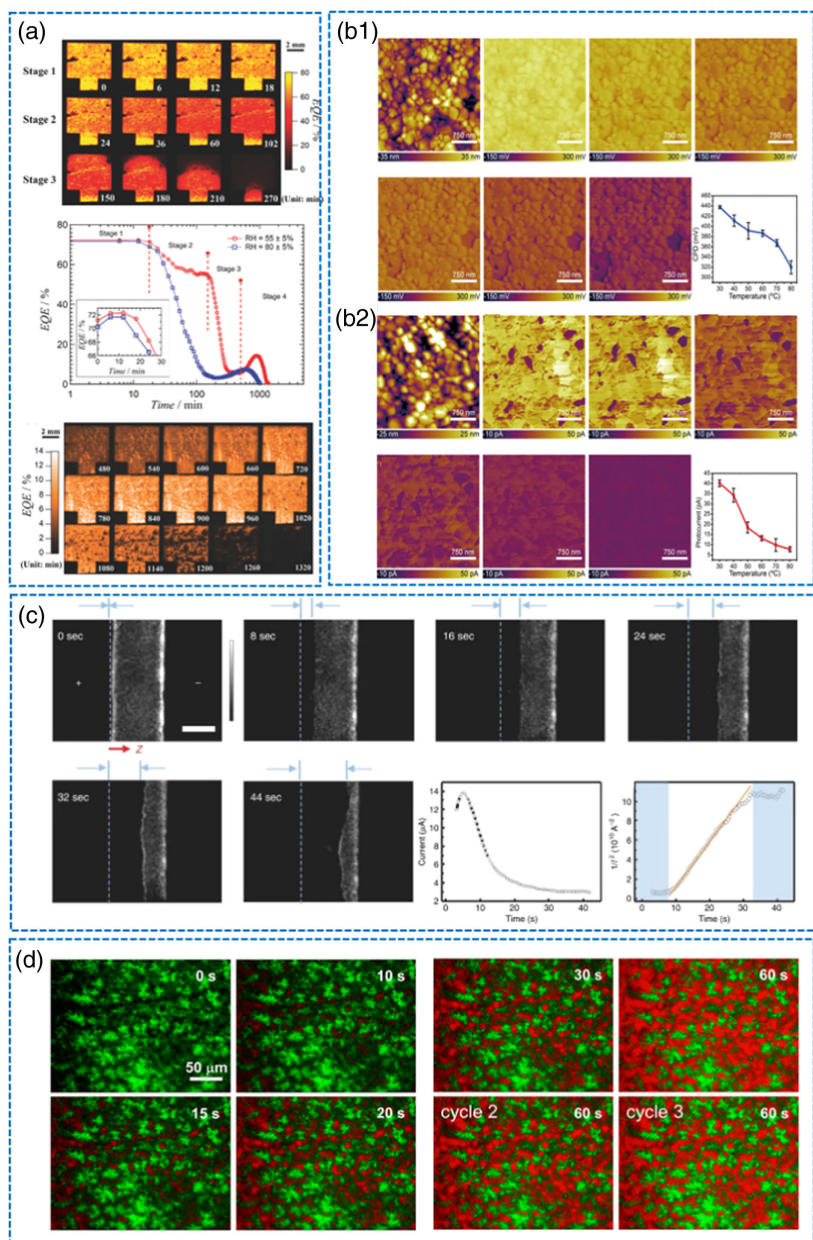


**Figure 7.** a) Light-beam-induced current (LBIC) EQE maps (at 532 nm) of a typical PSC after exposure at  $50 \pm 5\%$  RH (top). Areal average LBIC EQE (at 532 nm) as a function of time after exposure to humidity (middle). LBIC images for Stage 4 (480–1320 min) are shown with a higher resolution color scale (down). Reproduced with permission.<sup>[71]</sup> Copyright 2016, Wiley-VCH. b1) and b2) AFM topographic image of the MAPbI<sub>3</sub> films at 30 °C, and the corresponding contact potential difference (CPD) distributions of the MAPbI<sub>3</sub> films at 30, 40, 50, 60, 70, and 80 °C with the average CPD and photocurrent as a function of temperature. Reproduced with permission.<sup>[72]</sup> Copyright 2019, American Chemical Society. c) Time-dependent PL images of a perovskite film (MAPbI<sub>3-x</sub>Cl<sub>x</sub>) under an external electric field ( $\approx 2 \times 10^4$  V m<sup>-1</sup>). The “+” and “-” signs indicate the polarity of the electrodes. The excitation intensity is  $\approx 35$  mW cm<sup>-1</sup> with a wavelength of 440 nm, and the exposure time per image is 200 ms. The channel length is  $\approx 150$  μm.  $z(t)$  represents the PL-quenched areas. The color bar is a grey value with arbitrary units, indicating the PL intensity. Reproduced with permission.<sup>[73]</sup> Copyright 2018, Springer Nature. d) Optical microscopy photoluminescence photographs of a mixed-halide film kept under illumination. Reproduced with permission.<sup>[74]</sup> Copyright 2017, American Chemical Society. e) PL spectra of (MA)Pb(Br<sub>x</sub>I<sub>1-x</sub>)<sub>3</sub> thin films after illuminating for 5–10 min (10–100 mW cm<sup>-2</sup>, 457 nm) and PL spectra of an  $x = 0.6$  thin film after sequential cycles of illumination for 2 min (457 nm, 15 mW cm<sup>-2</sup>) followed by 5 min in the dark. Reproduced with permission.<sup>[75]</sup> Copyright 2015, Royal Society of Chemistry.

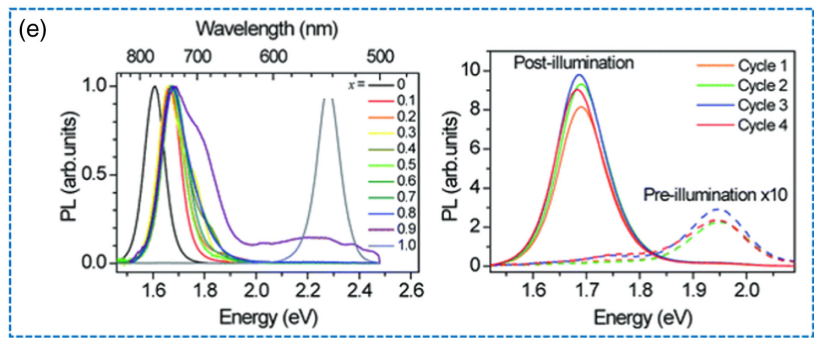


**Figure 7.** Continued.

information about the contact potential or work function of the PSCs surface, which helps to reveal the electrical related mechanism of PSCs. In Figure 7b1, Ma and coworkers<sup>[72]</sup> carried out the *in situ* KPFM to study the local morphology changes of  $\text{MAPbI}_3$  film as the temperature increased from 30 to 80 °C. The image field was kept constant, they calculated an average contact potential difference (CPD) on the square scanning area of  $\text{MAPbI}_3$ , which could help to evaluate the Fermi level shift dependent on temperature and the CPD of the films decreased with the increase of temperature gradually. As well, the average CPD declined with temperature increase was consistent with the temperature dependent of Fermi level of n-type semiconductor. This work affirms that thermal stressing would induce the phase transformation of perovskite and is consistent with the decline of photocurrent. To further figure out the carrier transportation and recombination in perovskite film, *in situ* atomic force microscope (AFM) was adopted to investigate the photocurrent distribution under illumination in the same temperature range, from 30 to 80 °C. Figure 7b2 shows that the average photocurrent also diminished with the temperature increasing. The shifted-down Fermi level caused the decrease of CPD and photocurrent, and it resulted in the decrease of the build-in field since the carriers were almost constant due to the impurity being completely ionized and the intrinsic excitation was not significant at this temperature range. Meantime, the lattice vibration scattering was the principal contradiction to increase the resistance for the carrier migration and as well reduced the carrier mobility. Thus, it is effective to understand the degradation mechanisms by utilizing the *in situ* KPFM and AFM to investigate the evolution of carrier dynamic migration during heat- and light-induced degradation processes. These *in situ* KPFM and AFM results exhibited the carries dynamics and migration process within devices under different stressing factors and helped to figure out the mechanism for devices performance changes.

*In situ* PL spectroscopy is a popular and widely used characterization technique for halide PSCs, especially for some wide-bandgap perovskite materials, which could offer observations for the recombination kinetics and the carrier dynamic. It is normally utilized to characterize the ion migration in mixed-halide PSC during the degradation process induced by the applied stress factors. For example, Li and coworkers carried out *in situ* PL to optically record the dynamical changes of  $\text{MAPbI}_{3-x}\text{Cl}_x$

perovskite film with symmetric electrodes, which was measured by a wide-field PL image microscope under a constant bias. As seen from Figure 7c, the PL intensity was suppressed gradually from the positively biased electrode, which may be caused by the migration of iodine vacancies under bias and the induced enhancement of non-radiative recombination.<sup>[73]</sup> Deng and coworkers also utilized *in situ* PL to investigate the ion migration in  $\text{MAPbI}_3$  perovskite film under light soaking. They found iodide vacancies would migrate to the interface, which would reduce charge-carrier separation and increase recombination.<sup>[28]</sup> The *in situ* characterization in the previous work dynamically displayed the whole ion migration process and verified that iodine vacancies would assist the ion migration under bias stressing within mixed-halide perovskite. These findings demonstrate the photoinduced degradation involved in ion migration through iodine vacancies and further understand for photoinduced degradation.

Recently, wide-bandgap PSCs have attracted much attention due to their application in multi-junction or tandem solar cells consisting of wide-bandgap top cells and narrow bandgap bottom cells.<sup>[74]</sup> Mixed I/Br wide-bandgap perovskite materials inherit intrinsic photo-instability due to the photoinduced halide segregation. Hoke and coworkers first discovered the mixed-halide  $\text{MAPb}(\text{I}_{1-x}\text{Br}_x)_3$ , ( $0.2 < x < 1$ ) perovskite tended to segregate into higher bandgap Br-rich and lower I-rich phases under continuous illumination, and these phases would behave as carrier traps to increase the recombination rate.<sup>[75]</sup> Therefore, the investigation for photoinduced phase segregation of wide-bandgap perovskite materials shows the importance of the study of the stability of wide-bandgap PSCs. Similarly, Marongiu and coworkers tracked the phase segregation caused by the light-induced ion migration through *in situ* PL with an optical microscope. Figure 7d showed the formation dynamics of phase segregation and visualized the iodide-rich domains at the surface.<sup>[76]</sup> *In situ* results visualized the phase segregation process compared with ex situ results and gave more details about the phase segregation degradation process. Hoke and coworkers found the PL peak shifted into low energy, and phase segregation induced the tails appearing in the PL spectra, as showed in Figure 7e.<sup>[75]</sup> These *in situ* PL phase segregation results were highly consistent with the previous results and the wide-bandgap perovskite indeed formed I-rich and Br-rich regions under continuous laser illumination. In addition to the MA-based film, the light-induced phase

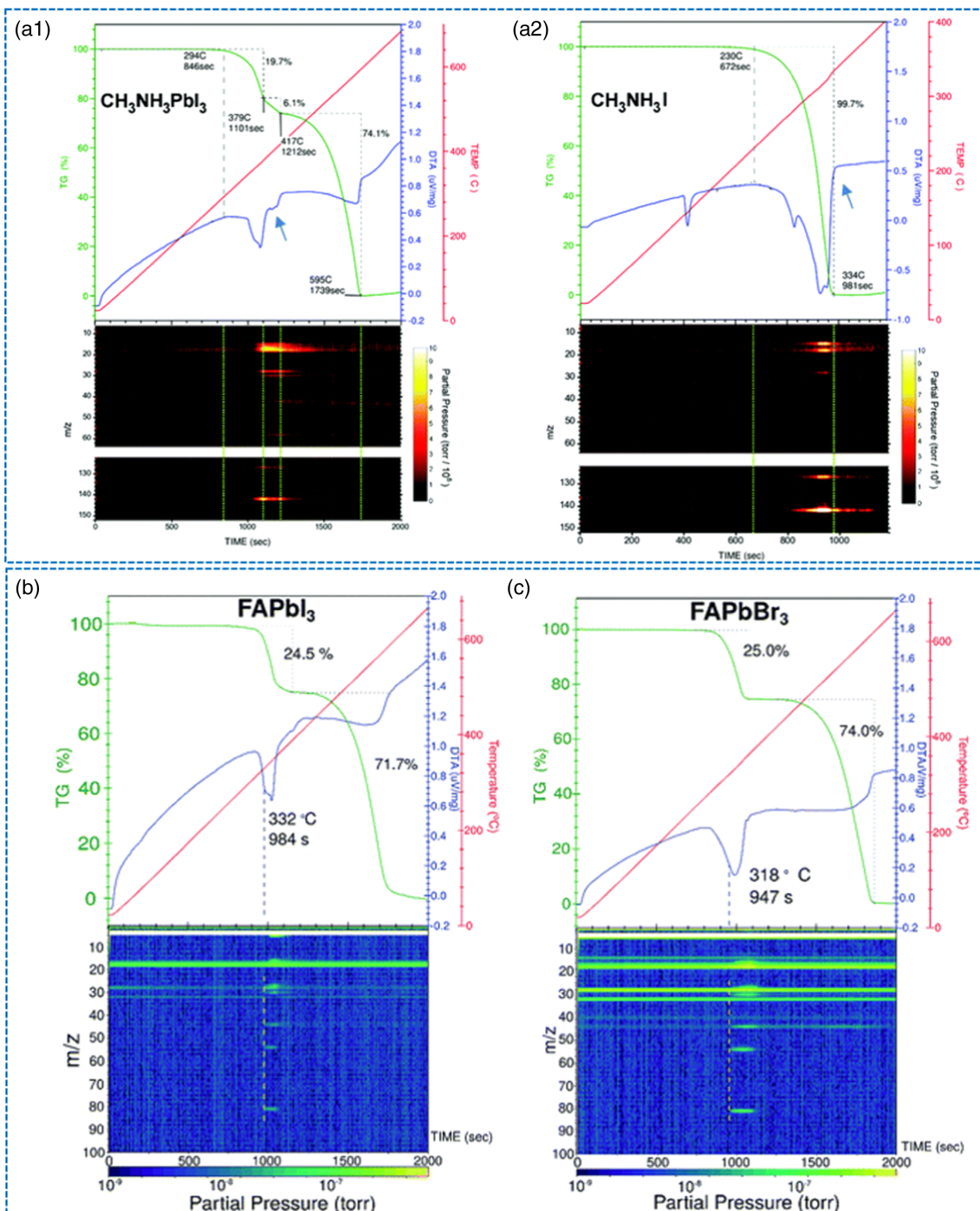


**Figure 8.** a1,a2) In situ thermal gravimetric and differential thermal analysis (TG-DTA) traces and the  $m/z$  peaks recorded simultaneously for MAPbI<sub>3</sub> and MAI during heating degradation (heating rate of  $20\text{ }^{\circ}\text{C min}^{-1}$ ). Blue arrows indicated the endothermic process in the DTA trace in MAPbI<sub>3</sub> perovskite but absent in the MAI salt. Reproduced with permission.<sup>[82]</sup> Copyright 2016, Royal Society of Chemistry. b,c) In situ TG-DTA coupled with mass spectrometry (MS) for FAPbI<sub>3</sub> and FAPbBr<sub>3</sub>, respectively. The top panels (green line) showed the archetypal two-step-type mass loss TG pattern for perovskite, bottom panels showed the MS traces recorded. Reproduced with permission.<sup>[83]</sup> Copyright 2019, Royal Society of Chemistry.

segregation of FACs-based film also has been studied by many studies.<sup>[67,77]</sup> Sutter-Fella and coworkers utilized in situ steady-state PL to compare different perovskites with I/Br ratio, including FACsPb(I<sub>0.8</sub>Br<sub>0.2</sub>)<sub>3</sub>, FACsPb(I<sub>0.5</sub>Br<sub>0.5</sub>)<sub>3</sub>, and

FACsPb(I<sub>0.4</sub>Br<sub>0.6</sub>)<sub>3</sub> under laser illumination. They found an additional PL peak from higher Br concentration ( $\text{Br} \geq 0.5$ ), which was attributed to the formation of the I-rich phase.<sup>[67]</sup> The in situ PL characterization compared the different ratios of I/Br and

proved that a high concentration of Br would exacerbate the phase segregation in wide-bandgap perovskite material. This finding indicated to the aforementioned works that ion migration under light or laser illumination would help to form the I-rich region and Br-rich region. Ma and coworkers presented similar PL peak redshift results of triple cation  $\text{Cs}_{0.05}(\text{FA}_{0.87}\text{MA}_{0.13})_{0.95}\text{Pb}(\text{I}_{0.87}\text{Br}_{0.13})_3$  perovskite film by in situ PL in the air under continuous one sun white light illumination and this redshift related with phase segregation.<sup>[77]</sup> Based on these in situ results, they also figured out that inserting a type of semiconducting organic ammonium cationic interface modifier between the light-harvesting perovskite film and the hole-transporting layer could effectively suppress ion migration and halide phase segregation.<sup>[77]</sup> Lately, many works have been attributed to handling this phase segregation within wide-bandgap PSCs.<sup>[78–80]</sup> In addition to the previous surface passivation,<sup>[77]</sup> Xu and coworkers found to utilize triple-halide alloys (Cl, Br, I) to tailor the bandgap and stabilize the phase segregation under

illumination.<sup>[80]</sup> Liang and coworkers demonstrated that potassium additive is effective to suppress photoinduced phase segregation for  $\text{FA}_{0.8}\text{Cs}_{0.2}\text{Pb}(\text{I}_{0.7}\text{Br}_{0.3})_3$  wide-bandgap perovskite material.<sup>[78]</sup> Because  $\text{K}^+$  can effectively suppress  $\text{I}^-$  diffusion through blocking the diffusion pathway and increase the energy of creating iodide vacancy.<sup>[81]</sup> These in situ PL results not only exhibit the photoinduced phase segregation degradation process for mixed-halide perovskite but also can act as a vital leading for suppressing phase segregation.

Based on these in situ findings, the valuable guidelines of mixed halide PSCs can be presented that using FA and Cs to replace MA as the A-site cation can stabilize the perovskite from phase segregation due to the reduction defect concentration, increasing the grains and lower-vacancy concentrations. The high content of Br would induce phase segregation in the I-rich region. Thus, a suitable I/Br ratio, adding Cl content and even incorporating potassium ions could eliminate phase segregation effectively based on these in situ results.

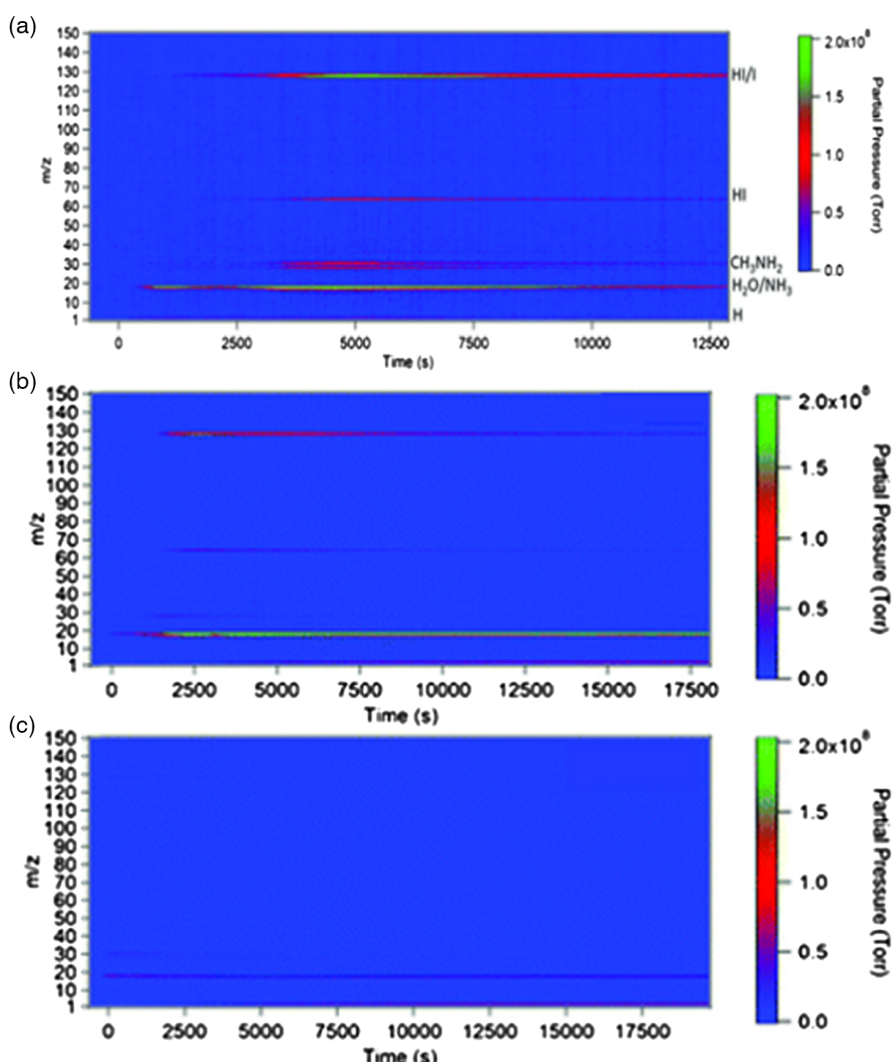


**Figure 9.** Time-resolved evolution of MS of the gas released during the photoinduced decomposition of a)  $\text{MAPbI}_3$ , b)  $\text{FAPbI}_3$ , and c)  $\text{FA}_{0.8}\text{Cs}_{0.2}\text{PbI}_3$  under a simulated irradiance. Reproduced with permission.<sup>[85]</sup> Copyright 2018, Royal Society of Chemistry.

## 2.4. Other In Situ Characterizations

In addition to the previous three categories of in situ characterization techniques, recently in situ thermal gravimetric and differential thermal analysis (TG-DTA) coupled with in situ quadrupole mass spectrometry (MS) have also been demonstrated to be advanced and precise methods to observe the in-time degradation dynamics of perovskite materials and PSCs. TG-DTA is a suitable technique to identify the mass loss directly from perovskite degradation, which can detect the endothermic and/or exothermic phase transitions and also can quantify the percentage of mass loss during the heating of the perovskite material. However, this technique does not characterize the chemical nature of the released gases. Thus, accompanying with another tool, MS, for the gas detection can exhaust from TG-DTA equipment to identify the molecular mass of the released gases. Utilizing these in situ methods to capture the intermediate degradation products and degradation dynamics would be necessary for revealing the degradation process of PSCs in time under thermal and photo stressing factors.

### 2.4.1. Heat

Utilizing in situ TG-DTA coupled with in situ MS effectively studies the thermal degradation of perovskite materials and PSCs. Juarez-Perez and coworkers utilized in situ TG-DTA coupled with quadrupole MS to characterize the thermal decomposition of MAPbI<sub>3</sub>. Unlike the standard decomposition MAPbI<sub>3</sub> into CH<sub>3</sub>NH<sub>2</sub> and hydrogen iodide (HI), they found that the significant decomposition gas products were CH<sub>3</sub>I and NH<sub>3</sub>. In Figure 8a1, a2, TG trace results for MAPbI<sub>3</sub> presented two consecutive mass loss steps: the first loss step ascribed to the nominal loss of MAI and the second loss step ascribed to the inorganic PbI<sub>2</sub> loss. The results also showed TG-DTA traces and the mass-to-charge ratio (*m/z*) peaks recorded simultaneously during the thermal degradation for MAPbI<sub>3</sub> and MAI. Contrary to expected results, *m/z* peaks for CH<sub>3</sub>NH<sub>2</sub> (methylamine [MA] *m/z* = 31) and HI (*m/z* = 128) gases were not detected during the thermal degradation of MAPbI<sub>3</sub> and MAI, but they detected the peaks which corresponded with NH<sub>3</sub> and CH<sub>3</sub>I.<sup>[82]</sup> The degradation reactions corresponded with the thermal reaction mentioned in Section 2 before.

Replacing MA<sup>+</sup> with organic cation FA<sup>+</sup> and metal cation Cs<sup>+</sup> can effectively improve thermal stability. Later, Juarez-Perez and coworkers studied the thermal stability of FA-based perovskite also by utilizing in situ TG-DTA coupled with MS. As is shown in Figure 8b,c, FAPbI<sub>3</sub> and FAPbBr<sub>3</sub> perovskite materials showed similar two-step mass loss traces, which indicated the loss of organic part of FA followed by the inorganic halide PbX<sub>2</sub> (X = Br and I) loss at above 400 °C.<sup>[83]</sup>

In situ TG-DTA and MS can identify the signature volatile products of the thermal decomposition of organic hybrid perovskite materials. Furthermore, these in situ results verify that MAPbI<sub>3</sub> would produce major decomposition gases under thermal stress: CH<sub>3</sub>I and NH<sub>3</sub>, which is different from the other thermal decomposition path: degrading into CH<sub>3</sub>NH<sub>2</sub> and HI. Compared with MA-based perovskite materials, FA-based perovskite materials show better thermal stability. Meanwhile,

incorporating Cs<sup>+</sup> also is an effective strategy to enhance the thermal stability of FA-based perovskites.

### 2.4.2. Light Illumination

In situ MS results can be useful evidence to verify the degradation dynamics of perovskite materials. For the photodecomposition of MAPbI<sub>3</sub> perovskite material, Juarez-Perez and coworkers still utilized in situ MS to present reversible and irreversible photodecomposition reactions of MAPbI<sub>3</sub> perovskite material. They summarized three degradation pathways that resulted from sunlight irradiation: first, MAPbI<sub>3</sub> degraded into CH<sub>3</sub>NH<sub>2</sub> and HI, which was identified as a reversible path, second, MAPbI<sub>3</sub> degraded into CH<sub>3</sub>I and NH<sub>3</sub>, which was identified as irreversible or detrimental path and the reversible third pathway, MAPbI<sub>3</sub> degraded into Pb(0) and I<sub>2</sub>(g). They found MAPbI<sub>3</sub> continuously released organic CH<sub>3</sub>NH<sub>2</sub>, HI, CH<sub>3</sub>I, and NH<sub>3</sub> under light illumination and vacuum conditions. They also found that the main difference between MAPbBr<sub>3</sub> and MAPbI<sub>3</sub> was that under vacuum and near room temperature conditions, MAPbI<sub>3</sub> showed numerous degradation gas products (CH<sub>3</sub>I, NH<sub>3</sub>, CH<sub>3</sub>NH<sub>2</sub>, HI, and I<sub>2</sub>); however, MAPbBr<sub>3</sub> only released CH<sub>3</sub>NH<sub>2</sub> and HBr. Yet under almost inert He pressure conditions and at a high temperature of almost 300 °C, both of them underwent similar degradation processes of releasing CH<sub>3</sub>I from MAPbI<sub>3</sub> or CH<sub>3</sub>Br from MAPbBr<sub>3</sub> and NH<sub>3</sub> gas, respectively.<sup>[84]</sup> Based on this in situ technique, they demonstrated dynamic processes of continuous photodecomposition of MAPbI<sub>3</sub> and MAPbBr<sub>3</sub> perovskite materials, which may aid tackle this stability problem.

Song and coworkers utilized in situ MS to present the photodegradation of MA- and FA-based perovskite materials. They used in situ MS to determine the chemical compositions of the gases released from MAPbI<sub>3</sub> under simulated solar irradiation. Figure 9a shows the evolution of the mass-to-charge ratio spectrum and a variety of gas species including H<sub>2</sub>, NH<sub>3</sub>, H<sub>2</sub>O, CH<sub>3</sub>NH<sub>2</sub>, HI, and I<sub>2</sub> were detected. By analyzing these results, the photodegradation dynamics of MAPbI<sub>3</sub> were determined.

Many studies suggest that replacing with less volatile organic cations FA<sup>+</sup> and metal cations Cs<sup>+</sup> would effectively enhance photostability. Thus, they operated in situ MS measurement on FAPbI<sub>3</sub> and FA<sub>0.8</sub>Cs<sub>0.2</sub>PbI<sub>3</sub> under a simulated irradiance and the FAPbI<sub>3</sub> results showed significantly lower emission of organic species in terms of CNH and CNH<sub>2</sub> in Figure 9b, but comparable HI emission compared with MAPbI<sub>3</sub>, which means the significant HI release could still limit the fundamental durability of FAPbI<sub>3</sub>. In contrast, incorporating Cs<sup>+</sup> into FAPbI<sub>3</sub> indeed suppressed the photodecomposition of perovskite materials. In Figure 9c, FA<sub>0.8</sub>Cs<sub>0.2</sub>PbI<sub>3</sub> showed two orders of magnitude less loss of materials during continuous illumination.<sup>[85]</sup>

## 3. Damage and Challenges in In Situ Characterization of Perovskite Solar Cells

As discussed previously, many characterizations techniques have been used for PSC stability study. However, due to the unique properties of perovskite material, such as the rapidly

photoinduced degradation and bias-induced degradation, the characterization tools face challenges to characterize these dynamic degradation processes.

The finding of electron beam damage has happened from the start of utilizing EM to characterize the PSCs. Although in some works, damage and defects from electron beam irradiation are designed for intended structural transformations.<sup>[20]</sup> However, in general, the source beam would damage the perovskite and worsen the degradation from measurements during *in situ* characterization, which is supposed to be avoided in characterization. Many works have discovered the electron beam damage in various perovskite materials and many reviews have covered the electron beam damage in different materials.<sup>[86,87]</sup> For example, the high-energy electron beam from *in situ* EM characterization would cause the formation of defects due to the irradiation damage and the transformation of phases due to the heating of the electron beam.<sup>[38]</sup> The electron-induced damage strongly depends on electron beam irradiation conditions.<sup>[88]</sup> Although *in situ* EM is a valuable technique to study the morphology changes of perovskite materials during degradation processes, the irradiation conditions should be carefully controlled to avoid any significant beam damage.

Recently, Ran and coworkers concluded three main interaction categories of electron beam damage in halide perovskites: displacement damage, ionization damage, and electrostatic charging damage.<sup>[89]</sup> First of all, displacement damage normally originates from the direct energy transferring from an electron of the electron beam to an atom in the samples when the energy exceeds the threshold of some displacement energy. Thus, it is vital to decline the characterization beam energy below the threshold of the displacing energy, so the displacement damage from the testing electron beam can be avoided. Undoubtedly, the threshold energy for a different type of perovskite materials is different, even varying from an atomic species to another atomic species in the same perovskite material, and from bulk atoms to surfaces or grain boundaries. It is important to figure out the energy threshold of the certain perovskite.

Then, ionization damage comes from the excitation and ionization of the specimen, which would result in the breaking of bonds and atomic displacement. This ionization damage is dependent on the materials and it will show up more probably than displacement damage. This damage energy transferred from a separate absorbed energy process mainly results from the thermal vibration. Lowering the electron beam is a simple way to alleviate the damage, but this change may affect the imaging condition for some perovskite materials.<sup>[90]</sup> So just cooling the samples can effectively reduce the defect rate. Thus, many cryogenic temperature-assisted characterizations have been utilized to alleviate this phase transformation (defect formation) or even degradation induced by this ionization damage. The biological community first employed cryogenic EM (cryo-EM) to visualize highly sensitive biological macromolecules<sup>[91]</sup> and soon this cryo-EM has been applied in different materials field, especially including perovskite materials.<sup>[27,92]</sup> Li and coworkers employed cryo-EM protocols to present the most original atomic-resolution imaging for the perovskite material MAPbI<sub>3</sub> under various conditions, which were impossible for the TEM to investigate the atomic structures for MAPbI<sub>3</sub> due to its extreme sensitivity to electron beam irradiation.<sup>[27]</sup> This cryogenic

temperature-assisted characterizations indeed preserve the authentic atomic structure to minimize this electron damage to a large extent by the designed freezing process. But the electron beam source and its dose are still a key tackle for electron beam damage. Latest, the biggest success in the application of a type cryo-FIB in the biology field has drawn much attention.<sup>[93]</sup> Traditional FIB can prepare samples with nanometer precision and extract the samples in a specific orientation with improved accuracy and efficiency for subsequent imaging work compared with other EM preparation methods. However, cryo-FIB operating at low temperature can be used to prepare perovskite samples in minimized damage. Combined with cryo-FIB preparation and cryo-EM imaging, the native states and structure of these perovskite samples can be observed. Although cryo-FIB has been more and more widely utilized in different fields in recent years, its potential for sample preparation of sensitive perovskite materials have not been demonstrated and verified thoroughly.

Another vital one is electrostatic charging damage. The electron beam in a large number of EM characterizations is transmitted through the perovskite specimen and nearly all the electrons would outlet from the backside of the specimen. Then, these electrons would excite the emission of secondary electrons and Auger electrons but within a nonconducting specimen, it would result in the buildup of a positive charge to form an electric field. Soon, the ionic bonds would be broken and then the free cations and anions would induce apparent structure changes under this strong electric field. It is recognized that electrostatic charging is highly dependent on both the electron beam dose and the exposure time of this beam.<sup>[89]</sup> So, return to the key question that establishing a standard definition of a critical electron dose and exposure time for a specific perovskite material is sincerely necessary.

Generally speaking, reducing the accelerating voltage and detecting the current of the electron beam to threshold energy and a critical dose, coupled with cryo-EM, cryo-FIB, and cryo-assisted characterizations, are more conducive to the characterization of *in situ* EM and beneficial to other technologies based on the electron beam.

As well, *in situ* X-Ray characterization requires a specific X-Ray source, such as the high-energy X-Ray source of synchrotron radiation, which quickly generates localized thermal vibration and light illumination interaction with perovskite material.<sup>[94,95]</sup> These X-Ray beam damages would induce artifacts during characterization.<sup>[96]</sup> Source beam radiation damage from X-Ray beam makes it challenging to explain the measurement results correctly due to the damage introduced artifacts in measured spectra, reflection, and imagines. Therefore, to correctly interpret the characterization results, it is necessary to evaluate and eliminate the damage of probe radiation to the perovskite material and devices.

To investigate the degradation processes induced by different factors, the measurement environment requires to change with the applied factors. Most apparatuses are equipped with sample chambers for *in situ* characterization to apply different simulated conditions. For *in situ* EM and some X-Ray and PL characterizations, the chambers are required to be under high vacuum. However, a high vacuum would damage the perovskite material and devices. Under high vacuum, the decomposition

products of perovskite would be pumped out by the pump system, which means the decomposition reactions are not easily kept equilibrium, affecting the study of degradation. Meanwhile, the high vacuum condition limits the usage of in situ EM to investigate the degradation with the existence of humidity and air.

#### 4. Conclusion and Outlook

In this work, we introduced advanced in situ characterization such as in situ EM, X-Ray, and optoelectronic tools, which have made considerable contributions in the targeted observation of perovskite materials and devices during degradation processes.

In situ EM could be valuable tools to observe the evolution of morphology changes during degradation induced by heat, light, and biasing. In collaboration with EDX, the structure changes and ion migration can also be tracked. It easily directly observed MAPbI<sub>3</sub> perovskite material degradation process dynamically and concluded the decomposition products during degradation based on the in situ EM results under heat stress. The better thermal stability of FA- and Cs-based perovskite material indeed showed a slower degradation rate when compared with MA-based perovskite material. Thus, the mixed FA/Cs perovskite material possesses better resistance to heat as stable devices. Nevertheless, mixed FA/Cs cation perovskite material stability under biasing stressing did not present apparent advantages compared with MA-based perovskite materials. Thus, more studies for in situ EM about different perovskite materials and devices are needed.

Meanwhile, there is still room for understanding the light-induced degradation process. The light-induced ion migration leading to phase segregation is a common degradation phenomenon for more stable FA/Cs mixed-cation mixed-halide perovskite materials and devices, and as well the phase segregation is mostly characterized by PL techniques. Hence, in situ EM would be an important tool in the future to study the light-induced degradation process and mechanism by visualizing this phase segregation dynamically and observing complete degradation processes directly. However, EM characterization requires high vacuum conditions due to the need of focusing on high-intensity electronic beams, thus utilizing in situ EM to observe the degradation in air or humidity is difficult to operate.

For in situ X-Ray-assisted characterization, the tools are various and can be operated in any environmental conditions. Thus, utilizing in situ X-Ray-assisted characterization can detect different perovskite under heat, humidity, and light even bias conditions. As the most commonly studied popular perovskite material MAPbI<sub>3</sub>, from in situ results of MAPbI<sub>3</sub> film under temperature elevating, it is easily found MAPbI<sub>3</sub> thermal unstable and degraded into PbI<sub>2</sub> causing irreversible degradation. Then replacing MA<sup>+</sup> cation of the perovskite material with FA<sup>+</sup>, Cs<sup>+</sup> cation or mixed two cations perovskite to improve thermal stability and in situ results of these mixed perovskite films prove that it did enhance crystallinity and structural stability. However, FAPbI<sub>3</sub> perovskite films own insufficient moisture stability compared with excellent thermal stability. Therefore, the mixed A-cation with FA<sup>+</sup> and/or Cs<sup>+</sup> perovskite films would improve the thermal and humidity stability. In a word, FA<sup>+</sup>- and

Cs<sup>+</sup>-based MA-free perovskites would enhance thermal and humidity stability and improve PSCs operation lifetime under humidity and heating condition. The result of in situ X-Ray-assisted characterization also found the phase segregation from different ratio halide anions or cations resulting from ion migration. Although in situ X-Ray characterizations are utilized to observe the time-resolved phase and structure changes, the ion migration and photoelectric properties of PSCs are supposed to be unachievable or need to use other characterizations.

The ion migration induced by humidity, heat, biasing, and illumination is responsible for the poor performance of PSCs. Thus, advanced in situ characterization to track the environmental factor-induced ion migration can help to better understand the PSCs degradation mechanism and help to solve these challenges. The application of in situ optoelectronic characterization, such as PL, LBIC KPFM, etc., can easily characterize the ion migration and phase segregation under light, heat, humidity, and even biasing. The optical photographs of the characterization can be observed more tangibly. The ion migration-induced phase segregation is a normal degradation phenomenon of perovskite films and devices under bias or illumination. From in situ PL results of mixed-cation halide perovskite, the I<sup>-</sup>/Br<sup>-</sup> anions are common choices of perovskite material but high content of Br would induce phase segregation to from I-rich region. Thus, a suitable I/Br ratio could eliminate phase segregation. Meanwhile, based on the in situ results, replacing MA<sup>+</sup> with FA<sup>+</sup>/Cs<sup>+</sup> as the A-site cation can stabilize the perovskite from phase segregation due to the reduction defect concentration, increasing the grains and lower-vacancy concentrations. Generally, to obtain wide-bandgap, FA<sup>+</sup> and Cs<sup>+</sup> mixed-cation perovskite with lower content of Br<sup>-</sup> would avoid the phase segregation of perovskite material films and loss of performance of mixed-cation PSCs to keep high PCE and stable operation performance, especially under working illumination.

Even more, we can observe the degradation processes and study the degradation mechanism of the perovskite solar modules (PSMs) through the in situ characterizations. Basically, the degradation of the active layers from PSMs under different stressing factors can be directly tracked assisting with the in situ techniques. These in situ tools also allow us to track the reaction between the perovskite layer and metal electrode in the PSMs in real time, especially to observe the perovskite degradation processes on the silverback electrode in the module. In addition, the ion migration between the interface layers and metal electrodes also can be observed in real time. The systematic establishment of module degradation mechanisms by in situ characterization is encouraged to assist investigators in improving module stability.<sup>[97]</sup>

Although fast developments have been made, in situ characterization meets various challenges. First, the high-energy beam would cause unavoidable damage due to the sensitivity of perovskite materials. Thus, the measurement conditions should be precisely controlled to eliminate the damage and artifacts, which would confound the degradation pathways and mechanism, no matter the high-intensity electronic beam and laser or synchrotron radiation X-Ray. Second, to obtain more accurate test results, the requirements for probe sources are severe. For example, synchrotron radiation should be applied for an in situ X-Ray characterization probe. Therefore, the proper and effective

source probe beams should be designed and implemented. Third, a suitable beam should be developed to be utilized in EM characterization to break through barriers that can only be tested in a high vacuum in the future. Utilizing more accurate in situ characterization to observe the degradation dynamically and systematically can better figure out the degradation pathway of moisture, heat, light, and biasing factors. However, convenient external encapsulation may avoid moisture- and air-induced degradation. Thus, if the photo-induced ion migration under biasing during degradation processes could be essentially investigated, researchers can easily make a positive breakthrough for stability and promote the development of industrialization for PSCs.

## Acknowledgements

X.M. and X.T. contributed equally to this work. This work was financially supported by the National Key Research and Development Project funding from the Ministry of Science and Technology of China (Grant No. 2021YFB3800104), the National Natural Science Foundation of China (51822203, 52002140, U20A20252, 51861145404, 62105293), Young Elite Scientists Sponsorship Program by CAST, the Self-determined and Innovative Research Funds of HUST (2020kfjXJJS008 and 2020KFYXJJS008), the Natural Science Foundation of Hubei Province (ZRMS2020001132), Shenzhen Science and Technology Innovation Committee (JCYJ20180507182257563), the Outstanding Young Talents Innovation Team Support Plan of Zhengzhou University and the Innovation Project of Optics Valley Laboratory (Grant No. OVL2021BG008).

## Conflict of Interest

The authors declare no conflict of interest.

## Keywords

degradation mechanism, dynamical observation, in situ techniques, ion migration, perovskite solar cells

Received: March 28, 2022  
Published online: May 1, 2022

- [1] U. Krishnan, M. Kaur, M. Kumar, A. Kumar, *J. Photonics Energy* **2019**, 9, 02001.
- [2] Y. Zhao, H. Tan, H. Yuan, Z. Yang, J. Z. Fan, J. Kim, O. Voznyy, X. Gong, L. N. Quan, C. S. Tan, J. Hofkens, D. Yu, Q. Zhao, E. H. Sargent, *Nat. Commun.* **2018**, 9, 1607.
- [3] H. S. Kim, J. Y. Seo, N. G. Park, *ChemSusChem* **2016**, 9, 2528.
- [4] A. Kojima, K. Teshima, Y. Shirai, T. Miyasaka, *J. Am. Chem. Soc.* **2009**, 131, 6050.
- [5] J. H. Im, C. R. Lee, J. W. Lee, S. W. Park, N. G. Park, *Nanoscale* **2011**, 3, 4088.
- [6] H. S. Kim, C. R. Lee, J. H. Im, K. B. Lee, T. Moehl, A. Marchioro, S. J. Moon, R. Humphry-Baker, J. H. Yum, J. E. Moser, M. Gratzel, N. G. Park, *Sci. Rep.* **2012**, 2, 591.
- [7] H. Hu, Z. Ren, P. W. K. Fong, M. Qin, D. Liu, D. Lei, X. Lu, G. Li, *Adv. Funct. Mater.* **2019**, 29, 1900092.
- [8] J. Jeong, M. Kim, J. Seo, H. Lu, P. Ahlawat, A. Mishra, Y. Yang, M. A. Hope, F. T. Eickemeyer, M. Kim, Y. J. Yoon, I. W. Choi, B. P. Darwich, S. J. Choi, Y. Jo, J. H. Lee, B. Walker, S. M. Zakeeruddin, L. Emsley, U. Rothlisberger, A. Hagfeldt, D. S. Kim, M. Gratzel, J. Y. Kim, *Nature* **2021**, 592, 381.
- [9] D. Ma, *J. Phys. Conf. Ser.* **2021**, 1865, 022078.
- [10] G. Niu, X. Guo, L. Wang, *J. Mater. Chem. A* **2015**, 3, 8970.
- [11] B. Salhi, Y. S. Wudil, M. K. Hossain, A. Al-Sulaiman, *Renewable Sustainable Energy Rev.* **2018**, 90, 210.
- [12] Z. Li, M. Yang, J.-S. Park, S.-H. Wei, J. J. Berry, K. Zhu, *Chem. Mater.* **2015**, 28, 284.
- [13] C. J. Bartel, C. Sutton, B. R. Goldsmith, R. Ouyang, C. B. Musgrave, L. M. Ghiringhelli, M. Scheffler, *Sci. Adv.* **2019**, 5, 0693.
- [14] L. T. Schelhas, Z. Li, J. A. Christians, A. Goyal, P. Kairys, S. P. Harvey, D. H. Kim, K. H. Stone, J. M. Luther, K. Zhu, V. Stevanovic, J. J. Berry, *Energy Environ. Sci.* **2019**, 12, 1341.
- [15] W.-J. Yin, T. Shi, Y. Yan, *Appl. Phys. Lett.* **2014**, 104, 063903.
- [16] S. P. Dunfield, L. Bliss, F. Zhang, J. M. Luther, K. Zhu, M. F. A. M. Hest, M. O. Reese, J. J. Berry, *Adv. Energy Mater.* **2020**, 10, 1904054.
- [17] N. Arora, M. I. Dar, M. Abdi-Jalebi, F. Giordano, N. Pellet, G. Jacopin, R. H. Friend, S. M. Zakeeruddin, M. Gratzel, *Nano Lett.* **2016**, 16, 7155.
- [18] Z. Li, C. Xiao, Y. Yang, S. P. Harvey, D. H. Kim, J. A. Christians, M. Yang, P. Schulz, S. U. Nanayakkara, C.-S. Jiang, J. M. Luther, J. J. Berry, M. C. Beard, M. M. Al-Jassim, K. Zhu, *Energy Environ. Sci.* **2017**, 10, 1234.
- [19] J. W. Lee, N. G. Park, *Adv. Energy Mater.* **2019**, 10, 1903249.
- [20] O. Dyck, M. Ziatdinov, D. B. Lingerfelt, R. R. Unocic, B. M. Hudak, A. R. Lupini, S. Jesse, S. V. Kalinin, *Nat. Rev. Mater.* **2019**, 4, 497.
- [21] M. Kodur, R. E. Kumar, Y. Luo, D. N. Cakan, X. Li, M. Stuckelberger, D. P. Fenning, *Adv. Energy Mater.* **2020**, 10, 1903170.
- [22] M.-C. Kim, N. Ahn, E. Lim, Y. U. Jin, Peter V. Pikhitsa, J. Heo, S. K. Kim, H. S. Jung, M. Choi, *J. Mater. Chem. A* **2019**, 7, 12075.
- [23] G. Abdelmageed, C. Mackeen, K. Hellier, L. Jewell, L. Seymour, M. Tingwald, F. Bridges, J. Z. Zhang, S. Carter, *Sol. Energy Mater. Sol. Cells* **2018**, 174, 566.
- [24] C. Das, M. Wussler, T. Hellmann, T. Mayer, W. Jaegermann, *Phys. Chem. Chem. Phys.* **2018**, 20, 17180.
- [25] M. L. Petrus, Y. Hu, D. Moia, P. Calado, A. M. Leguy, P. R. Barnes, P. Docampo, *ChemSusChem* **2016**, 9, 2699.
- [26] L. S. Dubrovinsky, S. K. Saxena, F. Tutti, S. Rekhi, T. LeBehan, *Phys. Rev. Lett.* **2000**, 84, 1720.
- [27] Y. Li, W. Zhou, Y. Li, W. Huang, Z. Zhang, G. Chen, H. Wang, G. H. Wu, N. Rolston, R. Vilà, W. Chiu, Y. Cui, *Joule* **2019**, 3, 2854.
- [28] X. Deng, X. Wen, J. Zheng, T. Young, C. F. J. Lau, J. Kim, M. Green, S. Huang, A. Ho-Baillie, *Nano Energy* **2018**, 46, 356.
- [29] R. S. Sanchez, E. Mas-Marza, *Sol. Energy Mater. Sol. Cells* **2016**, 158, 189.
- [30] H. Tsai, R. Asadpour, J. C. Blancon, C. C. Stoumpos, O. Durand, J. W. Strzalka, B. Chen, R. Verduzco, P. M. Ajayan, S. Tretiak, J. Even, M. A. Alam, M. G. Kanatzidis, W. Nie, A. D. Mohite, *Science* **2018**, 360, 67.
- [31] M.-C. Kim, N. Ahn, D. Cheng, M. Xu, S.-Y. Ham, X. Pan, S. J. Kim, Y. Luo, D. P. Fenning, D. H. S. Tan, M. Zhang, G. Zhu, K. Jeong, M. Choi, Y. S. Meng, *ACS Energy Lett.* **2021**, 6, 3530.
- [32] J. Chun-Ren Ke, A. S. Walton, D. J. Lewis, A. Tedstone, P. O'Brien, A. G. Thomas, W. R. Flavell, *Chem. Commun.* **2017**, 53, 5231.
- [33] M. I. Asghar, J. Zhang, H. Wang, P. D. Lund, *Renewable Sustainable Energy Rev.* **2017**, 77, 131.
- [34] Q. Jeangros, M. Duchamp, J. Werner, M. Kruth, R. E. Dunin-Borkowski, B. Niesen, C. Ballif, A. Hessler-Wyser, *Nano Lett.* **2016**, 16, 7013.
- [35] K. Song, L. Liu, D. Zhang, M. P. Hautzinger, S. Jin, Y. Han, *Adv. Energy Mater.* **2020**, 10, 1904006.

- [36] H. Sun, G. W. P. Adhyaksa, E. C. Garnett, *Adv. Energy Mater.* **2020**, *10*, 2000364.
- [37] G. Divitini, S. Cacovich, F. Matteocci, L. Cinà, A. Di Carlo, C. Ducati, *Nat. Energy* **2016**, *1*, 15012.
- [38] B. Yang, O. Dyck, W. Ming, M. H. Du, S. Das, C. M. Rouleau, G. Duscher, D. B. Geohegan, K. Xiao, *ACS Appl. Mater. Interfaces* **2016**, *8*, 32333.
- [39] J. A. Aguiar, S. Wozny, T. G. Holesinger, T. Aoki, M. K. Patel, M. Yang, J. J. Berry, M. Al-Jassim, W. Zhou, K. Zhu, *Energy Environ. Sci.* **2016**, *9*, 2372.
- [40] Z. Fan, H. Xiao, Y. Wang, Z. Zhao, Z. Lin, H.-C. Cheng, S.-J. Lee, G. Wang, Z. Feng, W. A. Goddard, Y. Huang, X. Duan, *Joule* **2017**, *1*, 548.
- [41] T. W. Kim, N. Shibayama, L. Cojocaru, S. Uchida, T. Kondo, H. Segawa, *Adv. Funct. Mater.* **2018**, *28*, 1804039.
- [42] D. Li, S. A. Bretschneider, V. W. Bergmann, I. M. Hermes, J. Mars, A. Klasen, H. Lu, W. Tremel, M. Mezger, H.-J. Butt, S. A. L. Weber, R. Berger, *J. Phys. Chem. C* **2016**, *120*, 6363.
- [43] B.-A. Chen, J.-T. Lin, N.-T. Suen, C.-W. Tsao, T.-C. Chu, Y.-Y. Hsu, T.-S. Chan, Y.-T. Chan, J.-S. Yang, C.-W. Chiu, H. M. Chen, *ACS Energy Lett.* **2017**, *2*, 342.
- [44] Y. Han, S. Meyer, Y. Dkhissi, K. Weber, J. M. Pringle, U. Bach, L. Spiccia, Y.-B. Cheng, *J. Mater. Chem. A* **2015**, *3*, 8139.
- [45] R. Wang, J. Xue, L. Meng, J.-W. Lee, Z. Zhao, P. Sun, L. Cai, T. Huang, Z. Wang, Z.-K. Wang, Y. Duan, J. L. Yang, S. Tan, Y. Yuan, Y. Huang, Y. Yang, *Joule* **2019**, *3*, 1464.
- [46] Y.-H. Seo, J. H. Kim, D.-H. Kim, H.-S. Chung, S.-I. Na, *Nano Energy* **2020**, *77*.
- [47] H. J. Jung, D. Kim, S. Kim, J. Park, V. P. Dravid, B. Shin, *Adv. Mater.* **2018**, *30*, 1802769.
- [48] H. Yuan, E. Debroye, K. Janssen, H. Naiki, C. Steuwe, G. Lu, M. Moris, E. Orgiu, I. H. Uji, F. De Schryver, P. Samori, J. Hofkens, M. Roeffaers, *J. Phys. Chem. Lett.* **2016**, *7*, 561.
- [49] J. M. Howard, R. Lahoti, M. S. Leite, *Adv. Energy Mater.* **2020**, *10*, 1903161.
- [50] F. U. Kosasih, C. Ducati, *Nano Energy* **2018**, *47*, 243.
- [51] K. H. Stone, A. Gold-Parker, V. L. Pool, E. L. Unger, A. R. Bowring, M. D. McGehee, M. F. Toney, C. J. Tassone, *Nat. Commun.* **2018**, *9*, 3458.
- [52] N. K. Kim, Y. H. Min, S. Noh, E. Cho, G. Jeong, M. Joo, S. W. Ahn, J. S. Lee, S. Kim, K. Ihm, H. Ahn, Y. Kang, H. S. Lee, D. Kim, *Sci. Rep.* **2017**, *7*, 4645.
- [53] K. W. Tan, D. T. Moore, M. Saliba, H. Sai, L. A. Estroff, T. Hanrath, H. J. Snaith, U. Wiesner, *ACS Nano* **2014**, *8*, 4730.
- [54] K. Meng, X. Wang, Q. Xu, Z. Li, Z. Liu, L. Wu, Y. Hu, N. Liu, G. Chen, *Adv. Funct. Mater.* **2019**, *29*, 1902319.
- [55] M. Qin, K. Tse, T. K. Lau, Y. Li, C. J. Su, G. Yang, J. Chen, J. Zhu, U. S. Jeng, G. Li, H. Chen, X. Lu, *Adv. Mater.* **2019**, *31*, 1901284.
- [56] W. Tan, A. R. Bowring, A. C. Meng, M. D. McGehee, P. C. McIntyre, *ACS Appl. Mater. Interfaces* **2018**, *10*, 5485.
- [57] J. Schlipf, L. Biessmann, L. Oesinghaus, E. Berger, E. Metwalli, J. A. Lercher, L. Porcar, P. Muller-Buschbaum, *J. Phys. Chem. Lett.* **2018**, *9*, 2015.
- [58] K. M. Fransishyn, S. Kundu, T. L. Kelly, *ACS Energy Letters* **2018**, *3*, 2127.
- [59] F. Valipour, E. Yazdi, N. Torabi, B. F. Mirjalili, A. Behjat, *J. Phys. D* **2020**, *53*, 285501.
- [60] Y. Hu, M. F. Aygüler, M. L. Petrus, T. Bein, P. Docampo, *ACS Energy Lett.* **2017**, *2*, 2212.
- [61] Q. Lu, Z. Yang, X. Meng, Y. Yue, M. A. Ahmad, W. Zhang, S. Zhang, Y. Zhang, Z. Liu, W. Chen, *Adv. Funct. Mater.* **2021**, *31*, 2100151.
- [62] X. Tang, M. Brandl, B. May, I. Levchuk, Y. Hou, M. Richter, H. Chen, S. Chen, S. Kahmann, A. Osvet, F. Maier, H.-P. Steinrück, R. Hock, G. J. Matt, C. J. Brabec, *J. Mater. Chem. A* **2016**, *4*, 15896.
- [63] A. Senocrate, T. Acartürk, G. Y. Kim, R. Merkle, U. Starke, M. Grätzel, J. Maier, *J. Mater. Chem. A* **2018**, *6*, 10847.
- [64] J.-W. Lee, D.-H. Kim, H.-S. Kim, S.-W. Seo, S. M. Cho, N.-G. Park, *Adv. Energy Mater.* **2015**, *5*, 1501310.
- [65] G. Niu, W. Li, J. Li, X. Liang, L. Wang, *RSC Adv.* **2017**, *7*, 17473.
- [66] T. Singh, T. Miyasaka, *Adv. Energy Mater.* **2018**, *8*, 1700677.
- [67] C. M. Sutter-Fella, Q. P. Ngo, N. Cefarin, K. L. Gardner, N. Tamura, C. V. Stan, W. S. Drisdell, A. Javey, F. M. Toma, I. D. Sharp, *Nano Lett.* **2018**, *18*, 3473.
- [68] U. B. Cappel, S. Svanstrom, V. Lanzilotto, F. O. L. Johansson, K. Aitola, B. Philippe, E. Giangrisostomi, R. Ovsyannikov, T. Leitner, A. Fohlisch, S. Svensson, N. Martensson, G. Boschloo, A. Lindblad, H. Rensmo, *ACS Appl. Mater. Interfaces* **2017**, *9*, 34970.
- [69] T. Kirchartz, J. A. Márquez, M. Stolterfoht, T. Unold, *Adv. Energy Mater.* **2020**, *10*, 1904134.
- [70] F. Babbe, C. M. Sutter-Fella, *Adv. Energy Mater.* **2020**, *10*, 1903587.
- [71] Z. Song, A. Abate, S. C. Watthage, G. K. Liyanage, A. B. Phillips, U. Steiner, M. Graetzel, M. J. Heben, *Adv. Energy Mater.* **2016**, *6*, 1600846.
- [72] J. Y. Ma, J. Ding, H. J. Yan, D. Wang, J. S. Hu, *ACS Appl. Mater. Interfaces* **2019**, *11*, 21627.
- [73] C. Li, A. Guerrero, S. Huettner, J. Bisquert, *Nat. Commun.* **2018**, *9*, 5113.
- [74] M. Hu, C. Bi, Y. Yuan, Y. Bai, J. Huang, *Adv. Sci.* **2016**, *3*, 1500301.
- [75] E. T. Hoke, D. J. Slotcavage, E. R. Dohner, A. R. Bowring, H. I. Karunadasa, M. D. McGehee, *Chem. Sci.* **2015**, *6*, 613.
- [76] D. Marongiu, X. Chang, V. Sarritzu, N. Sestu, R. Pau, A. Geddo Lehmann, A. Mattoni, F. Quochi, M. Saba, A. Mura, G. Bongiovanni, *ACS Energy Lett.* **2017**, *2*, 769.
- [77] K. Ma, H. R. Atapattu, Q. Zhao, Y. Gao, B. P. Finkenauer, K. Wang, K. Chen, S. M. Park, A. H. Coffey, C. Zhu, L. Huang, K. R. Graham, J. Mei, L. Dou, *Adv. Mater.* **2021**, *33*, 2100791.
- [78] J. Liang, C. Chen, X. Hu, Z. Chen, X. Zheng, J. Li, H. Wang, F. Ye, M. Xiao, Z. Lu, Y. Xu, S. Zhang, R. Yu, C. Tao, G. Fang, *ACS Appl. Mater. Interfaces* **2020**, *12*, 48458.
- [79] L. Wang, G. Wang, Z. Yan, J. Qiu, C. Jia, W. Zhang, C. Zhen, C. Xu, K. Tai, X. Jiang, S. Yang, *Sol. RRL* **2020**, *4*, 2000098.
- [80] J. Xu, C. C. Boyd, Z. J. Yu, A. F. Palmstrom, D. J. Witter, B. W. Larson, R. M. France, J. Werner, S. P. Harvey, E. J. Wolf, W. Weigand, S. Manzoor, M. van Hest, J. J. Berry, J. M. Luther, Z. C. Holman, M. D. McGehee, *Science* **2020**, *367*, 1097.
- [81] J. Cao, S. X. Tao, P. A. Bobbert, C. P. Wong, N. Zhao, *Adv. Mater.* **2018**, *30*, 1707350.
- [82] E. J. Juarez-Perez, Z. Hawash, S. R. Raga, L. K. Ono, Y. Qi, *Energy Environ. Sci.* **2016**, *9*, 3406.
- [83] E. J. Juarez-Perez, L. K. Ono, Y. Qi, *J. Mater. Chem. A* **2019**, *7*, 16912.
- [84] E. J. Juarez-Perez, L. K. Ono, M. Maeda, Y. Jiang, Z. Hawash, Y. B. Qi, *J. Mater. Chem. A* **2018**, *6*, 9604.
- [85] Z. Song, C. Wang, A. B. Phillips, C. R. Grice, D. Zhao, Y. Yu, C. Chen, C. Li, X. Yin, R. J. Ellingson, M. J. Heben, Y. Yan, *Sustainable Energy Fuels* **2018**, *2*, 2460.
- [86] R. F. Egerton, P. Li, M. Malac, *Micron* **2004**, *35*, 399.
- [87] R. F. Egerton, *Micron* **2019**, *119*, 72.
- [88] O. Hentz, Z. Zhao, S. Gradelak, *Nano Lett.* **2016**, *16*, 1485.
- [89] J. Ran, O. Dyck, X. Wang, B. Yang, D. B. Geohegan, K. Xiao, *Adv. Energy Mater.* **2020**, *10*, 1903191.
- [90] D. Zhang, Y. Zhu, L. Liu, X. Ying, C. E. Hsiung, R. Sougrat, K. Li, Y. Han, *Science* **2018**, *359*, 675.
- [91] M. Adrian, J. Dubochet, J. Lepault, A. W. McDowall, *Nature* **1984**, *308*, 32.

- [92] X. Wang, Y. Li, Y. S. Meng, *Joule* **2018**, 2, 2225.
- [93] A. Rigort, J. M. Plitzko, *Arch. Biochem. Biophys.* **2015**, 581, 122.
- [94] R. L. Z. Hoye, P. Schulz, L. T. Schelhas, A. M. Holder, K. H. Stone, J. D. Perkins, D. Vigil-Fowler, S. Siol, D. O. Scanlon, A. Zakutayev, A. Walsh, I. C. Smith, B. C. Melot, R. C. Kurchin, Y. Wang, J. Shi, F. C. Marques, J. J. Berry, W. Turnas, S. Lany, V. Stevanović, M. F. Toney, T. Buonassisi, *Chem. Mater.* **2017**, 29, 1964.
- [95] A. M. A. Leguy, Y. Hu, M. Campoy-Quiles, M. I. Alonso, O. J. Weber, P. Azarhoosh, M. van Schilfgaarde, M. T. Weller, T. Bein, J. Nelson, P. Docampo, P. R. F. Barnes, *Chem. Mater.* **2015**, 27, 3397.
- [96] J. D. McGettrick, K. Hooper, A. Pockett, J. Baker, J. Troughton, M. Carnie, T. Watson, *Mater. Lett.* **2019**, 251, 98.
- [97] Z. Yang, Z. Liu, V. Ahmadi, W. Chen, Y. B. Qi, *Sol. RRL* **2021**, 6, 2100458.



**Zonghao Liu** received his B.Sc. in 2011 and Ph.D. in 2016 from Huazhong University of Science and Technology (HUST), China. He was a visiting student in University of California, Los Angeles, USA, in 2015. From 2016 to 2017, he was a research assistant in Peking University, China. From 2017–2019, he worked as a postdoctoral scholar at Okinawa Institute of Science and Technology Graduate University in Japan. He is currently an associate professor in Wuhan National Laboratory for Optoelectronics of HUST. His current research focuses on optoelectronics devices based on inorganic/organic perovskites, especially on perovskite solar cells.



**Wei Chen** received his B.S. and Ph.D. degrees from the Department of Materials Science and Engineering, Tsinghua University. He worked as a postdoctoral fellowship with the Department of Chemistry, Hong Kong University of Science and Technology, from 2008 to 2010. He was a visiting scholar with the National Institute for Materials Science, Japan, from 2014 to 2015. He is currently a professor with the Wuhan National Laboratory for Optoelectronics, Huazhong University of Science and Technology. His research interests cover the synthesis, understanding, and applications of functional nanomaterials and semiconductor thin films in next-generation solar cells, including PSCs.